Thesis for The Degree of Licentiate of Engineering

Experimental investigations of ageing of commercial BEV Li-ion batteries

Kristian Frenander

Department of Electrical Engineering
Chalmers University of Technology | University of Gothenburg
Gothenburg, Sweden, 2023

Experimental investigations of ageing of commercial BEV Li-ion batteries

Kristian Frenander

ISSN 1652-876X

Department of Electrical Engineering
Division of Electrical Engineering
Chalmers University of Technology | University of Gothenburg
SE-412 96 Göteborg,
Sweden
Phone: +46(0)31 772 1000

Printed by Chalmers Digitaltryck,
Gothenburg, Sweden 2023.

Till Hilda och Johanna

Experimental investigations of ageing of commercial BEV Li-ion batteries

Kristian Frenander

Department of Electrical Engineering
Division of Electrical Power Engineering
Chalmers University of Technology

Abstract

The rapid development of lithium-ion batteries has enabled changes in widespread applications ranging from portable electronics to electric vehicles and large scale grid energy storage. However, battery ageing remain a challenge in all these applications, and this thesis seeks to contribute to the understanding of Li-ion battery degradation.

In the compiled works, results from extensive testing on discharge current frequency, variation in SOC level and temperature are reported for cells with mixed material negative electrodes (Graphite/SiO_x). Unexpected trends where cycling in low SOC causes more rapid degradation than cycling in high SOC are observed. The capacity retention after 1200 FCE was 84.7% for cells cycled in 5-15% SOC, whereas for cells cycled in 45-55% SOC the capacity retention after 1200 FCE was 94.7%. This dependency is shown to be stronger than the temperature dependency for mixed material negative electrodes. It is also demonstrated that dynamic current profiles affect the capacity retention with a strong correlation for frequencies below 100 mHz.

The ageing processes involved are analysed using various in situ electrochemical characterisation techniques and post-mortem investigations. The strong SOC dependency is shown to be largely attributed to ageing of SiO_x in mixed material electrodes, with LAM_{SiO_x} contributing to a loss of 7% of overall capacity in 5-15% SOC cycling, compared to only 3% in 85-95% SOC cycling. For 0-50% SOC cycling in 45 °C temperature, capacity retention of SiO_x had dropped to $\sim$ 25 % of initial capacity, whereas graphite capacity was still in excess of 90% of initial capacity.

Keywords

Lithium Ion Batteries; Electric Vehicles; State of Charge; ageing; NCA; silicon oxide; lithium plating; Physics-based modelling; lifetime

List of Publications

Appended publications

This thesis is based on the following publications:

[**Paper I**] K. Frenander, T. Thiringer, *Low Frequency Influence on Degradation of Commercial Li Ion Battery*
Submitted, under review.

[**Paper II**] N. Roy Chowdhury, A.J. Smith, K. Frenander, A. Mikheenkova, R. Wreland Lindström, T. Thiringer, *The state of charge dependence of degradation in lithium-ion cells from a Tesla model 3*
Submitted, under review.

[**Paper III**] A. Mikheenkova, A.J. Smith, K. Frenander, Y. Tesfamhret, N. Roy Chowdhury, Cheuk-Wai Tai, T. Thiringer, R. Wreland Lindström, M. Hahlin, M.J. Lacey, *Ageing of High Energy Density Automotive Li-ion Batteries: The Effect of Temperature and State-of-Charge*
Submitted, under review.

Acknowledgment

I would like to thank my family and friends for their continuous and understanding support in achieving this milestone. A special thank you to my partner Johanna for being there for me through all of this work, I love you. I also direct a special thank you to my parents, not just for giving me a sense of curiosity and eagerness to learn, but also for all the help making it possible to actually write a thesis with a one-year-old at home. And of course a special thank you to Hilda for lighting up every day of my life for the last year and a half.

I am also extremely grateful for the help and guidance I have received from my main supervisor Torbjörn Thiringer, who despite a very busy schedule has always made time for questions, thoughts and discussions. Without your support this would not have been possible. A big thank you also to my co-supervisor Bertrand Philippe for the support and for helping me understand the fine details of the inner workings of a battery. Furthermore a special thank you to Johan Fridner for helping make this project possible and guiding me through the first year of it. And for showing me how get fast on the bike as well as in the lab. Thank you also to Patrik Johansson for guidance and input and for welcoming me into your research group, it has meant a lot for this project.

Thank you to all of the colleagues at both Volvo Cars and Elkraftteknik at Chalmers for nice company and interesting discussions along the way. A special thanks to Zeyang Geng, Evelina Wikner and Niladri Roy Chowdhury for all of the help and fruitful discussions.

Then I would also like to send a special thank you to Alex Smith, KTH, and Anastasiia Mikheenkova, Uppsala University, for the excellent collaboration on the two papers included in this thesis. I have learned so much from you in this project, and I'm very grateful for all your help.

And last but not least the financial support from Energimyndigheten (P48031-1) and Volvo Car Corporation is gratefully acknowledged.

Contents

List of Abbreviations

ANOVA analysis of variance

BOL beginning of life

CC constant current

CCCV constant current, constant voltage

DEC diethyl carbonate

DFN Doyle-Fuller-Newman

DMC dimethyl carbonate

DVA differential voltage analysis

EC ethylene carbonate

EDS energy-dispersive X-ray spectroscopy

EIS electrochemical impedance spectroscopy

EMC ethyl methyl carbonate

EOL end of life

EV electric vehicle

FCE full cycle equivalent

HOMO highest occupied molecular orbital

ICA incremental capacity analysis

ICI intermittent current interruption

ICP-OES inductively coupled plasma - optical emission spectroscopy

LAM loss of active material

LFP lithium iron phosphate

LIB lithium-ion battery

LLI loss of lithium inventory

LMO lithium manganese oxide

LUMO lowest unoccupied molecular orbital

NCA lithium nickel cobalt aluminium oxide

NCM lithium nickel cobalt aluminium oxide

OCV open circuit voltage

P2D pseudo-two-dimensional

PC polypropylene carbonate

RPT reference performance test

SEI solid electrolyte interphase

SEM scanning electron microscopy

SOC state of charge

TEM transmission electron microscopy

TM transition metal

TMO transition metal oxide

XRD X-ray diffraction

Mathematical symbols

List of Symbols - Electrochemical context

α	Transfer coefficient
β	Bruggeman coefficient
ϵ	Volume fraction
η	Overpotential in redox reaction, V
σ	Conductivity, $\mathrm{S\,m^{-1}}$
ϕ	Electrochemical potential, V
a	Area, $\mathrm{m^2}$
c	Lithium ion concentration, $\mathrm{mol\,m^{-3}}$
D	Diffusion coefficient, $\mathrm{m^2\,s^{-1}}$
E	Voltage, V
F	Faraday constant, $96\,485\,\mathrm{A\,s\,mol^{-1}}$
f_A	Activity coefficient of salt in electrolyte
i	Current density, $\mathrm{A\,m^{-2}}$
I	Full cell current, A
i_0	Exchange current density, $\mathrm{A\,m^{-2}}$
k	Reaction rate constant, $\mathrm{m\,s^{-1}}$
n	Number of electrons in redox reaction
Q	Cumulative capacity, A h
R	Gas constant, $8.314\,\mathrm{J\,mol^{-1}\,K}$
r	Radial distance in particle, m
R_p	Particle radius, m
T	Temperature, K
t	Time, s
t_+^0	Lithium ion transference number
U	Voltage, V

List of Symbols - Statistical context

α	Variance between subsets
ϵ	Noise estimation
μ	Mean value
df	Degrees of Freedom
E	Expected value
H	Statistical hypothesis
MS	Mean Squares
SS	Sum of Squares

Subscripts

a	Anodic
c	Cathodic
ct	Charge transfer
eff	Effective
eq	Equilibrium
l	Liquid electrolyte phase
Li	Plated lithium
neg	Negative electrode
pos	Positive electrode
ref	Reference
s	Solid phase

Part I

Extended Summary

Chapter 1

Introduction

1.1 Background

With growing awareness of the urgent need to de-carbonise the economy in general, and the transportation and power sectors in particular, the lithium-ion battery (LIB) has come to the forefront of the battle against climate change. The transport sector is a major emitter of carbon dioxide as 23% of total man-made CO_2 emissions worldwide coming from the transport sector [1], and the road sector contributes 74.5% of those emissions [2]. Thus the potential for reducing CO_2 emissions through vehicle electrification is significant.

Having emerged as the dominant energy storage technology chosen by the vehicle industry when shifting to electric propulsion LIBs are seen as a key technology for a green economy. This has led to large investments being directed into LIB technology in recent years. This has among other things lead to a 70% cost reduction in the decade between 2010 and 2020 [3], yet the battery remains the most expensive component in an electric vehicle (EV) [4] making it a key component in making EVs more affordable in order to continue increasing market penetration and reduce tailpipe emissions.

Furthermore batteries are large and heavy with a relatively large environmental footprint, especially when produced from pristine materials [5]. Their size and weight make them inconvenient and expensive to replace, further strengthening the emphasis put on the durability of EV batteries as a key factor for reducing both life-cycle cost and environmental load from LIBs.

To improve the lifetime of LIBs both the ageing mechanisms and the usage conditions that trigger them need to be better understood. To achieve this requires both better modelling abilities as well as better and more efficient testing procedures, which is what this thesis seeks to contribute to.

1.2 Previous Work

The increased market penetration of LIBs has meant that the understanding of how Li ion batteries age has become a field of major interest. Numerous studies

have been performed to investigate the influence of static parameters such as C-rate [6], [7], State of Charge (SOC) levels [8], [9], temperature [10]–[12] or combinations thereof [13]–[15]. But fairly limited research has gone into understanding the importance of dynamic usage given it is the modus operandi for all electric vehicles. Dynamic cycles derived from driving are tested in [15]–[18] and duty cycles from other dynamic applications in [19], [20]. Among the studies focusing on dynamic ageing, only a few had a reference test of similar current. Out of those that have, the reported influence of dynamics vary from significant in [15] to small impact (except for low temperature) in [16]. While all these works have proven insightful and contributed to the understanding of ageing processes, the amount of stochasticity in the real life operation of batteries and the large variation of results based on battery chemistry [13] means that further work is needed to enable optimal design of lifetime testing, as well as achieving a good understanding of the influence on ageing from usage parameters.

The use of large testing matrices that is required to discern the influence of specific usage parameters comes with some natural drawbacks, it is expensive and it takes a long time to get results. This, together with the great value of being able to simulate various usage profiles and reduce time to results, has led to an increase in interest for modelling degradation of LIBs. The modelling is mainly divided into two tracks

1. Empirical modelling
2. Physical modelling

where the empirical model approach uses data from a test matrix to fit parameters in a model directly correlating usage to degradation, without attributing it to specific chemical processes. Examples of such models can be found in [21]–[24]. Furthermore some authors have attempted to correlate the statistical model to the ageing processes in the battery, see [25], [26]. Lately however, with the development of physics-based models and increasing knowledge of parameters needed for example for the Doyle-Fuller-Newman (DFN) model there has been an increasing shift in interest towards physical modelling.

Physical models in this context mean that in addition to the desired redox reactions associated with normal battery operate, also the side reactions are explicitly modelled by extending an ideal physical model, typically the DFN model. This was pioneered by Arora, Doyle and White [27] who focused on Li plating and has since then been complemented with solid electrolyte interphase (SEI) models [15], [28]–[30], refined Li plating models [31]–[34] and most recently combinations thereof with explicit coupling between reactions [35].

In order to calibrate and verify models, there is still a fair amount of testing needed, but with increasing experience on parameter estimations and more publicly available datasets, for example through LiionDB [36], the accuracy of the predictions from physical ageing models should increase without increasing testing effort. As these models and methods are still in relatively early stages of development all contributions to model development and parametrisation testing is highly valuable.

1.3 Purpose

The purpose of the project is to further the understanding of ageing of LIBs, both by investigating influence of cycling conditions, and by investigating the ageing processes that occur during cycling by both non-invasive and post-mortem techniques. The knowledge generated should also help the development of ageing models, both empirical and physical.

Specifically the project focuses on investigating the influence of dynamic usage, as compared to constant current testing conditions, with the purpose of showing efficient and manageable ways to include this in lifetime assessment of commercial batteries. Utilising this kind of test methodology could possibly save test time and resources needed for comprehensive investigation of ageing behaviour.

1.4 Contributions to State of the Art

The main project contributions found in this thesis are:

- Development and implementation of test methods that take dynamic usage into account with few governing parameters.
- Providing ageing data for commercial cells with a mixed negative electrode and a nickel rich NCA positive electrode.
- Demonstrating that not taking dynamics into account in lifetime cycle testing, will affect the results, and could lead to erroneous conclusions.
- The degradation of electrodes with SiO_x and graphite blend show a strong SOC dependence, with a fast initial capacity fade for cycling in low SOC.
- Demonstrating that non-invasive characterisation methods can be sufficient to show heterogeneity in ageing of individual materials in mixed material electrode.
- Development of hysteresis analysis as tool to qualitatively assess the individual ageing of SiO_x and graphite in mixed negative electrode.

1.5 Thesis Outline

This thesis is arranged in the following way: Chapters 2 to 4 contain the studies presented in the appended papers, presenting theory for LIBs, ageing processes, and details on the experimental techniques utilised in the study. Moreover the results from the studies investigating how the state of charge (SOC) levels and dynamic discharge currents affect the ageing of LIBs.

Chapter 5 presents results from a so far unpublished study, focusing on pulse charge currents of various frequencies and their influence on the ageing of LIBs. Model work to interpret test results is also presented in this chapter.

Chapter 6 and 7 present the conclusions of the study and suggested future work.

Chapter 2

Theory

2.1 Lithium-ion Battery

Batteries, and electrochemical cells in general, are composed of two electrodes, one positive with higher potential and one negative with lower potential. One part of the redox (reduction/oxidation) reaction of the full cell will happen at each electrode, meaning that electrons are yielded at one electrode and consumed at the other. In a battery, by electrically insulating the electrodes while maintaining ionic connection through an electrolyte, the electrons involved in the redox reaction are forced to travel through an external circuit and thus produce electrical work in an external system. Thus the battery can work as an energy source for applications such as electric vehicles, consumer electronics, power tools etc.

The term *lithium-ion battery* specifically denotes electrode material pairings that operate with Li^+ as the positive mobile ionic species, meaning that Li^+ is the positive ion carrying current through the electrolyte to maintain charge balance while electrons carry the current in the external circuit. Nearly all currently available commercial LIBs are of insertion type, where the Li is inserted into a host structure where it diffuses into free sites and is stored until next cycle, but metallic electrodes also exist. The host structure enables reversibility of the process as Li^+ can be inserted and removed repeatedly making the battery rechargeable. The ion transfer between electrodes can happen either spontaneously from negative to positive electrode (discharge) or driven by an external electrical voltage from positive to negative electrode (charge).

In Fig. 2.2 a cross-section of the battery is schematically represented with its most important components and the electron and Li^+ flow during discharge. The main components are:

1. Positive current collector. Typically manufactured from aluminium.

2. Positive electrode. Commonly a transition metal oxide, often with high Nickel content, such as $LiNi_aCo_bAl_cO_2$ (NCA) or $LiNi_aCo_bMn_cO_2$

(NCM) where $a + b + c = 1$ and $a \approx 0.85$. Other common materials include $LiFePO_4$ (LFP) and $LiMnO_2$ (LMO) [5].

3. Separator. Ensures electrical insulation while permitting ionic transport, typically this is achieved with a polymer soaked in electrolyte [37].

4. Negative electrode. Until recently pure graphite was dominant as negative electrode material, but in recent years blended electrodes with graphite and silicon oxides SiO_x. For this study the focus will be solely on blended negative electrodes. Lithium titanium oxide (LTO) can also be found in commercial applications.

5. Negative current collector. Nearly exclusively made of copper due to stability issues at the low potential.

To facilitate ion and mass transfer the entire separator-electrode-stack is soaked in electrolyte. For almost all of the commercially available LIBs today the electrolyte is in liquid form, and while some examples of solid electrolytes exist they are outside the scope of this study. The liquid electrolytes are typically designed using a Li salt, normally $LiPF_6$, in solution in a mixture of different carbonates. Some of the most commonly used are dimethyl carbonate (DMC), ethylene carbonate (EC), ethyl methyl carbonate (EMC) and diethyl carbonate (DEC) but further compounds are also common. The carbonates are combined in different ratios to design electrolytes with different properties. Other chemical additives are also added to improve the performance of the battery [38].

Furthermore the electrolyte needs to be stable over a wide potential range, due to significant potential differences between the positive and negative electrodes. As the electrolyte is in direct contact with the electrodes it must withstand the reductive and oxidative potential of the electrodes [39].

When Li^+ shuttles back and forth between electrodes during operation of the battery, the concentration of Li in the respective electrode changes, changing the available energy in the battery. To track the amount of charge available to the user of the battery the quantity state of charge is defined. It is indicating how much capacity is available to discharge from the battery, ideally correlating to the amount of Li stored in each electrode. As the actual concentration in the host structures is not measurable in an operational battery it is typically tracked via the open circuit voltage (OCV), the voltage of the battery when there is no current flowing. The SOC is defined between 0% and 100% based on the OCV interval that the battery can be operated in. The correlation between SOC and OCV is graphically represented in Fig. 2.1.

2.2 Modelling of Li-ion Batteries

2.2.1 Doyle Fuller Newman Model

The most established model for calculating and describing the internal behaviour of Li Ion Batteries is the DFN model, proposed by the three researchers the

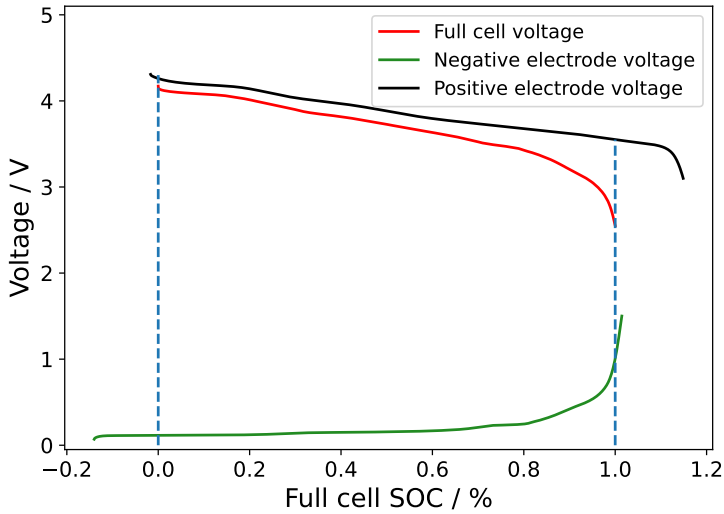

Figure 2.1: Open circuit voltages of full cell, positive electrode and negative electrode plotted versus SOC for the full cell. Note that unused capacity of electrodes extend outside 0 and 100% full cell SOC.

model is named after in a series of papers in the early nineties [40]–[42]. The equations used in the model are summarised in Table 2.1, with the different processes occurring in the battery shown in Fig. 2.2.

The central concepts of the DFN model is to use Butler-Volmer equation, see Equation 2.5, to model the charge transfer reaction happening at the electrode surface. In this equation the exchange current density is determined by Equation 2.6. The solid state diffusion in the electrode material is modelled by Fick's law, see Equation 2.1, while mass transfer and concentration in electrolyte are modelled utilising concentrated electrolyte theory, see Equation 2.3 and Equation 2.2. To account for the effects of porosity on the transport parameters porous electrode theory is applied using the Bruggeman correction, see Equation 2.4, where the value of correction factor β can vary to account for morphology, but is typically set around 1.5.

The DFN model can also be augmented to include non-ideal behaviour and side reactions [35], making it a popular choice for researchers focusing on battery ageing.

2.3 Ageing in Li-ion Batteries

The operation of LIBs described in Section 2.1 is however an idealised version only including the sought after intercalation reactions, and ignoring the possible unwanted side reactions, which are what makes batteries age.

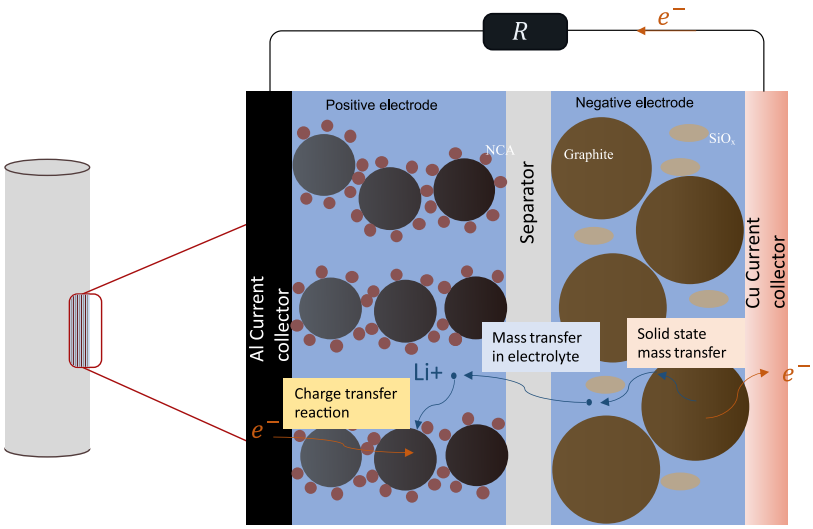

Figure 2.2: Graphic summary of physical processes in battery during discharge and their connection to the DFN model. Li^+ ions are released from the negative electrode, in pairs with electrons, in a charge transfer reaction. They are then separated and electrons transported through external circuit while Li^+ transport happens through the liquid electrolyte as mass transfer. Li^+ and electrons then combine in charge transfer reaction on positive electrode surface and diffuse to a free site in the porous electrode via solid state mass transfer.

Table 2.1: Summary of equations as used in the DFN model.

Process	Equation
Solid state mass transfer	$\frac{\partial c_s}{\partial t} = \frac{D_{s,eff}}{r^2}\frac{\partial}{\partial r}\left(r^2\frac{\partial c_s}{\partial r}\right)$ (2.1)
	$\left.\frac{\partial c}{\partial r}\right\|_{r=0} = 0 \qquad D_s \left.\frac{\partial c_s}{\partial r}\right\|_{r=R_p} = i/Fa_s$
Mass transfer in electrolyte	$\epsilon\frac{\partial c_l}{\partial t} = \nabla \cdot D_{l,eff}\nabla c - \frac{\boldsymbol{i}_l t_+^0}{F}$ (2.2)
	$\boldsymbol{i}_l = -\sigma_{l,eff}\nabla\phi_l + \left(\frac{2\sigma_{l,eff}RT}{F}\right)\left(1+\frac{\partial \ln f_A}{\partial \ln c_l}\right)\left(1-t_+^0\right)\nabla \ln c_l$ (2.3)
	$\sigma_{l,eff} = \sigma_l\epsilon_l^\beta \qquad D_{l,eff} = D_l\epsilon_l^\beta$ (2.4)
Charge transfer reaction	$i = i_0\left(\exp\left(\frac{\alpha_a nF}{RT}\eta\right) - \exp\left(-\frac{\alpha_c nF}{RT}\eta\right)\right)$ (2.5)
	$i_0 = Fk_{ct}\left(c_{s,max} - c_{s,surf}\right)^{\alpha_a} c_l^{\alpha_a} c_{s,surf}^{\alpha_c}$ (2.6)
	$\eta = E_{ct} - E_{eq}$

Ageing phenomena in Lithium Ion Batteries have been discussed extensively in the scientific literature, with overviews performed in for instance [43]–[46], where the authors have concluded that the main degradation comes from four unwanted side reactions.

- SEI growth
- Lithium plating
- Particle cracking in active material
- Positive electrode decomposition

In the following sections each of these will be explained in more detail.

2.3.1 SEI Growth

A layer of electrochemically passivating compounds needs to be formed on the surface of the graphite anode, since all commonly used electrolytes are unstable at potentials below 0.8 V *vs.* Li/Li^+ [47] and graphite electrodes are operated well below this threshold (typically down to ~ 0.05 V *vs.* Li/Li^+). This means that where graphite electrode and electrolyte come in direct contact a redox reaction will occur in which the different carbonates and the Li^+ in the electrolyte react with electrons from the electrode to form solids on the negative electrode material[48], [49]. These solids then form a protective layer on the negative electrode stabilising the system to lessen further reduction of electrolyte. Therefore the SEI layer can be said to be both a blessing and a curse since its existence helps stabilise the negative electrode and enables

the usage of graphite as negative electrode operating at low potential, but it also irreversibely consumes Li , meaning that cycling capacity is lost upon SEI formation. The properties of the SEI will also have a significant influence on how the battery ages, as the permeability of Li^+ to migrate through the SEI layer is an important factor in determining cell impedance.

The main formation of SEI will occur in the first cycles of a fresh battery, but since the SEI layer is somewhat porous to allow for Li^+ migration it will continue to grow continuously throughout the batteries service life. The exact mechanism through which SEI growth happens has not been fully clarified, but an overview by Single, Latz and Horstmann [28] found that four long term growth regimes are suggested in literature:

(a) Diffusion of solvent/salt through SEI pores.

(b) Electron tunneling through inner layer of SEI.

(c) Electron conduction through SEI.

(d) Diffusion of neutral radicals, typically Li interstitials.

where (a) assume SEI to be sufficiently porous for larger solvent molecules to reach electrode surface, (b) assume sufficient porosity for solvent molecules to reach within tunnelling distance ($\approx$2 nm [50]) from the electrode. Electron conduction (c) makes no assumptions about porosity, but requires non-zero electrical conductivity of the SEI. Neutral radical diffusion (d) assumes mobility of neutral species, namely Li , through the SEI. The growth modes are graphically presented in Fig. 2.3.

As the process bottleneck is transport processes driven by concentration gradients rather than overpotentials its occurrence is not limited to duty cycling, but will also occur during storage where cells are not subjected to any load. This makes SEI growth particularly interesting in EV applications where vehicles are known to be parked in excess of 90% of the time [51], making SEI a likely main contributor to degradation of EV batteries.

The thickness of the SEI layer is however also affected by the cycling conditions. During the intercalation process, graphite will expand and contract causing mechanical stress to the SEI layer. This can in turn lead to crack formation and breakage in the SEI. If the cracks are deep enough they can expose pristine electrode material to electrolyte and thus cause further formation of SEI and corresponding capacity loss.

2.3.2 Lithium Plating

Lithium plating is another degradation process occurring on the negative electrode due to operation at low potential, where Li^+ from the electrolyte form metallic Li on the electrode surface rather than intercalate into the electrode. It happens when the intercalation process is slower than the charging process leading to the current being split into an intercalation and a plating current [52]. This can happen for two main reasons

1. Local saturation of graphite electrode.

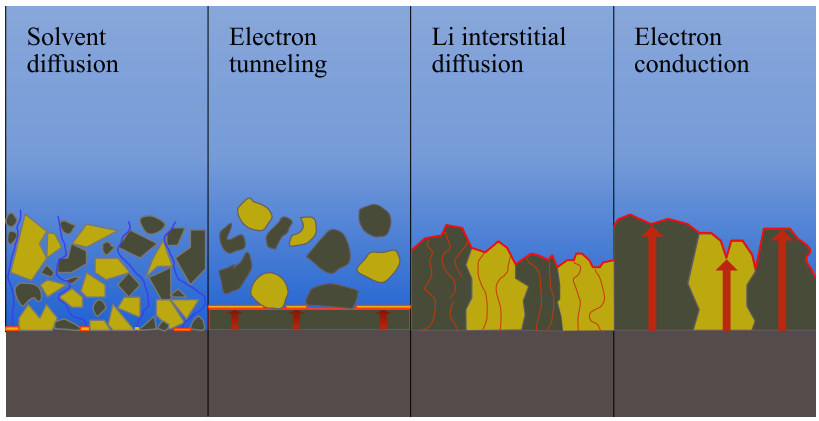

Figure 2.3: Schematic illustration of the four suggested growth models detailed in Section 2.3.1. Red and orange indicate regions where SEI growth is happening, arrows and curves indicate transport of species involved in reaction

2. Kinetically driven due to negative overpotential.

Local saturation can happen due to slow intercalation meaning that surface layers of graphite are full despite overall concentration in particles are not critical. This is often caused by low temperatures and/or fast charging. Saturation can also happen due to overcharging where the graphite is near saturation throughout, which reduces the rate of diffusion.

The kinetically driven process occurs when, despite concentrations of hosted Li being below maximum, the overpotential of the Li plating reaction, $\eta = \phi_s - \phi_l$, drops below 0 V *vs.* Li/Li^+. Here η denotes the reaction overpotential, ϕ_s denotes solid phase potential and ϕ_l denotes liquid phase potential. This means that the reduction of Li^+ to metallic Li on the particle surface becomes thermodynamically favourable. The conditions for this to occur are similar to those for local saturation with low temperature and fast charging being main causes for a drop in negative electrode potential and rise in liquid phase potential. For a schematic visualisation of Li plating, see Fig. 2.4.

Lithium plating is, just like all metallic electroplating reactions, reversible with the reverse reaction dubbed "Lithium stripping". However in a battery, SEI is formed on the plated Li if exposed to electrolyte due to the low potential (0 V *vs.* Li/Li^+ by definition). This can cause the metallic Li to become electrically isolated making it permanently lost to cycling. Isolated Li covered in SEI is denoted as *dead lithium*. This process means that lithium plating can only be said to be partially reversible and causes irreversible capacity loss.

One further way that plated Li can be recovered is by subsequent insertion into the electrode regardless of external current [53]. This is assuming that there are available sites in the electrode host structure, meaning that plating has not occurred due to overcharge.

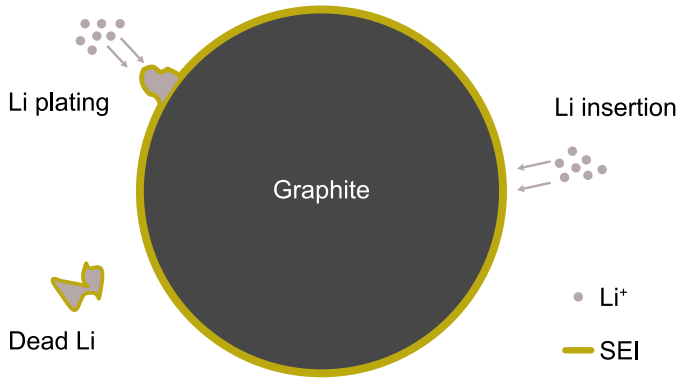

Figure 2.4: Visual schematic of processes involved in Li plating.

2.3.2.1 Modelling Lithium Plating

The plating and stripping of Li can be modelled as a kinetically limited process, meaning that it is governed by a Butler-Volmer equation. Since Li is not abundant on the electrode surface a concentration dependence must also be included in the model to avoid unlimited Li stripping occurring in normal operation. The concentration dependent Butler-Volmer equation can be written as

$$i_{Li} = i_{0,Li}\left(\frac{c_{Li}}{c_{Li,ref}}\exp\left(\frac{\alpha_a F\eta}{RT}\right) - \frac{c_l}{c_{l,ref}}\exp\left(-\frac{\alpha_c F\eta}{RT}\right)\right). \tag{2.7}$$

The concentration c_{Li} denotes the concentration of metallic Li and is calculated by solving the differential equation $\frac{\partial c_{Li}}{\partial t} = \frac{i_{Li}}{F}$ and $c_{Li,ref}$ denotes a reference concentration of plated Li , and is used as tuning parameter in most published work [31], [35]. The concentration of Li^+ in electrolyte is denoted as c_l, and $c_{l,ref}$ denotes the reference concentration in electrolyte. In the Butler-Volmer equation R is the gas constant, F is the Faraday constant, T denotes temperature and $\alpha_{a/c}$ denotes anodic and cathodic transfer coefficients respectively. The exchange current density of the plating reaction, $i_{0,Li}$, is calculated as $i_{0,Li} = Fk_{Li}c_{l,ref}c_{Li,ref}$, where k_{Li} is the kinetic rate constant and the overpotential of the reaction is $\eta = \phi_s - \phi_l$. When η is positive, the anodic reaction of Li stripping is kinetically favourable, and when η is negative the cathodic Li plating reaction dominates.

2.3.3 Particle Cracking

As mentioned in Section 2.3.1 the intercalation and de-intercalation processes causes alternating mechanical stresses in the electrode materials. The repeated stresses can in turn cause material fatigue and crack formation and propagation [54].

This contributes to capacity loss not only through re-formation of SEI consuming cyclable Li , but in extreme cases the cracks can cause parts of particles to become electrically disconnected from the rest of the electrode. This leads both to a loss of active material that can host Li and to the loss of the Li that is intercalated in the portion of the electrode particle that is disconnected [43].

2.3.4 Positive Electrode Decomposition

As mentioned in Section 2.1 most commercially available positive electrode are transition metal oxides (TMOs) which are susceptible to ion dissolution and migration and irreversible detrimental changes to the crystal structure. Layered oxides (for example lithium nickel cobalt aluminium oxide (NCM) and lithium nickel cobalt aluminium oxide (NCA)) can experience irreversible phase changes where the crystal structure decompose to disordered spinel or rock salt phases which are not capable of hosting intercalating Li . This can happen on entire surface layers of particles creating a passivating layer making the particle inaccessible to cycling, or locally with corresponding loss of active material. This process is accelerated at high potential/low lithiation [55].

Furthermore the transition metal in the positive electrode material can react with the electrolyte if highly oxidised nickel comes in contact with electrolyte. This causes electrolyte decomposition and the Ni ions can migrate to the negative electrode and form passivating surface film [46].

2.4 Characterisation Techniques

In this section a theoretical background is provided for the main charachterisation methods implemented in the studies is provided.

2.4.1 Incremental Capacity Analysis (ICA)

Incremental capacity is the derivative of cumulative capacity with respect to voltage, expressed mathematically as

$$ICA = \frac{\mathrm{d}Q}{\mathrm{d}U}. \tag{2.8}$$

This is useful as the voltage of an electrochemical cell is an expression of the chemical potential of the system, which follows Gibbs' phase rule, meaning that the slope of the chemical potential is corresponding to degrees of freedom in the thermodynamic system. As such, the voltage curve will exhibit plateaus and slopes corresponding to the solid state phases, and the transitions between them in the material. Plateaus on the voltage curve show up as peaks on the incremental capacity analysis (ICA) plot, and correspondingly slopes will show as valleys on an ICA plot. Voltage plateaus will be present when two or more phases coexist at the same potential, thus indicating a phase change between stages of lithiation for the electrode materials [56].

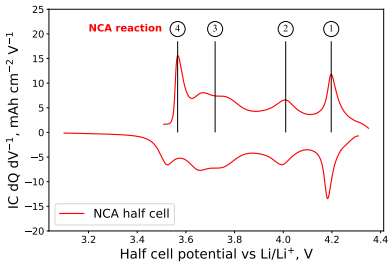

(a)

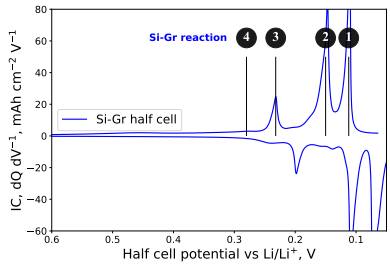

(b)

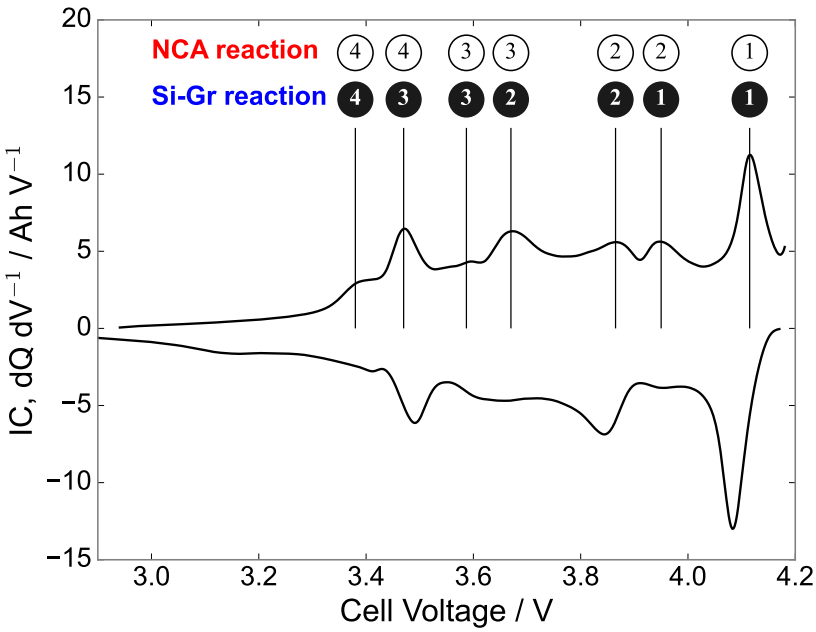

(c)

Figure 2.5: ICA on charge and discharge of each electrode and a full, cylindrical cell at BOL. Electrodes are harvested and reassembled into half cells and cycled at C/10: (a) NCA/Li, (b) Gr-SiO_x/Li. (c) NCA/Gr-SiO_x full cell at C/20. Reproduced and adapted from **Paper II**.

An example of the method is shown in Fig. 2.5, where ICA on individual electrodes with peaks marked is combined with full cell ICA, where the combined cell peaks are marked according to the electrode they originate from. For details on the phase transitions and methodology see **Paper II**.

By tracing the intensity of individual peaks as well as the distance between peaks, the ageing of individual electrodes can be assessed. In order for the slope of the voltage curve to be dominated by the material OCV curve, overpotentials in the incremental capacity test need to be low. Therefore these tests are performed at low C-rates (<C/10 for energy optimised cells) for clearer results.

2.4.2 Differential Voltage Analysis (DVA)

Differential voltage is the inverse of incremental capacity, being defined as the derivative of voltage with respect to cumulative capacity: $^{\mathrm{d}U}/_{\mathrm{d}Q}$. The main advantage of differential voltage analysis (DVA) relative to ICA is that the analysis is performed relative to capacity. This makes it possible to track the individual electrode capacity by tracking distances between peaks during cycling, making it a powerful tool for assessing electrode ageing.

As the voltage of the cell is the difference of positive and negative electrode potential

$$U_{cell}(Q) = U_{pe}(Q) - U_{ne}(Q). \tag{2.9}$$

The derivative of the full cell voltage is the sum of the derivatives of the individual electrode potentials

$$\frac{\mathrm{d}U_{cell}}{\mathrm{d}Q_{cell}} = \frac{\mathrm{d}U_{pe}}{\mathrm{d}Q_{pe}} + \left(-\frac{\mathrm{d}U_{ne}}{\mathrm{d}Q_{ne}}\right). \tag{2.10}$$

This makes the assignment of peaks more intuitive since the individual electrodes and full cell can be made to share x-axis with relatively simple scaling, which enables accurate electrode balancing, see Fig. 2.6. From this Figure it can also be noted that capacity values can be calculated based on distances between peaks, which can then be used as trackers for the individual material ageing.

2.4.3 Hysteresis Analysis

It is reported in literature that SiO_x produces large hysteresis between charge and discharge voltage at the same lithiation [57], [58]. In mixed materials electrodes this can be utilised to investigate the relative activity of SiO_x by calculating the hysteresis between charge and discharge voltage at the same SOC

$$U_{hyst} = U_{chrg} - U_{dchg}. \tag{2.11}$$

If this is calculated using data from low current galvanostatic cycling the influence from overpotentials can be minimised and a good approximation of the voltage hysteresis of the material can be obtained. A large hysteresis is thus indicative of SiO_x being the electrochemically active species and a smaller hysteresis indicates that lithiation is occurring mainly in graphite.

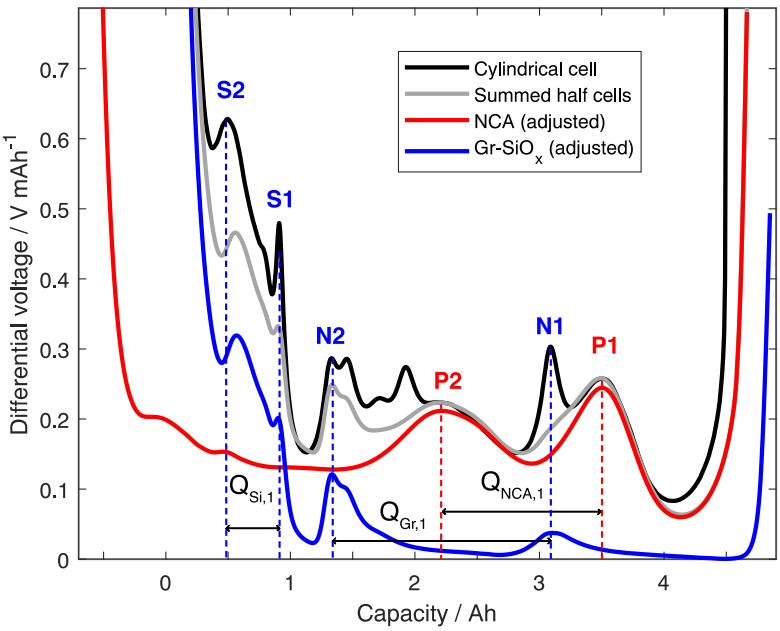

Figure 2.6: DVA for each electrode combined with full cell for the Panasonic 2170 cell described in Table 3.1. Individual electrode DVA has been scaled by size and unused end capacity to achieve peak fitting, which allows assigning full cell peaks to corresponding half cell peak. Dashed lines mark material peaks that are used to trace capacity retention of materials during cycling. Reproduced and adapted from **Paper II**.

2.5 Analysis of Variance (ANOVA)

The analysis of variance is a commonly implemented statistical tool to discern between noise and signal in a dataset. This is achieved by testing whether differences found between measurements can be explained from variance with a reasonable probability [59]. This implies finding the probability of a null hypothesis of all subset means of the dataset being equal

$$H_0 : \mu_1 = \cdots = \mu_n$$

versus the alternative hypothesis that a difference exists,

$$H_1 : \mu_i \neq \mu_j \text{ for some (i, j)}.$$

The foundation of ANOVA is the decomposition of any sampled data into three parts, overall mean, set variance and error. For example, consider a total of N samples from I individual subsets, with n samples from each dataset such that $N = I \cdot n$. Then a unique sample k from subset i, denoted as Y_{ik}, can be decomposed as

$$Y_{ik} = \mu + \alpha_i + \epsilon_{ik}, \qquad \epsilon_{ik} \sim N(0, \sigma). \tag{2.12}$$

The parameters can be estimated from the data as

$$\hat{\mu}_i = \overline{y}_{i\cdot} = \frac{1}{n} \sum_k y_{ik} \tag{2.13a}$$

$$\hat{\mu} = \overline{y}_{\cdot\cdot} = \frac{1}{N} \sum_k \sum_i y_{ik} \tag{2.13b}$$

$$\hat{\alpha}_i = \overline{y}_{i\cdot} - \overline{y}_{\cdot\cdot} \tag{2.13c}$$

where the dot notation implies average, such that $\overline{y}_{i\cdot}$ is the average for all observations from subset i.

This decomposition means that a dataset with no significant difference between subsets would have a low value of α compared to ϵ, and conversely for a dataset with significant differences. To test this a decomposition of the total sum of squares is defined as

$$SS_T = SS_A + SS_E$$

with

$$SS_T = \sum_i \sum_k \left(y_{ik} - \overline{y}_{\cdot\cdot}\right)^2, \qquad \mathrm{df_T} = N - 1 \tag{2.14a}$$

$$SS_A = n \sum_i \hat{\alpha}_i^2, \qquad \mathrm{df_A} = I - 1 \tag{2.14b}$$

$$SS_E = \sum_i \sum_k \hat{\epsilon}_{ik}^2, \qquad \mathrm{df_E} = I(n-1). \tag{2.14c}$$

Essentially this splits the variation in overall response between the variation in all groups (SS_E) and variation between subsets (SS_A). By normalising the

Table 2.2: Examples of outcomes and interpretations of an ANOVA test on hypothetical experimental studies.

I	n	F	$P(F \mid H_0)$	Interpretation and comment.
10	2	5	0.03	H_0 can be rejected with 97% probability. Typically considered as significant.
10	2	0.5	0.37	H_0 can be rejected with 63 % probability. Typically considered as non-significant, although graphic inspection might indicate trend.
7	60	3	0.082	H_0 can be rejected with 91.8 % probability. Typically considered as non-significant as a minimum of 95% probability is required.

sum of squares by degree of freedom we obtain a directly comparable metric, denoted as *mean squares*

$$MS_A = \frac{SS_A}{\mathrm{df_A}} \tag{2.15a}$$

$$MS_E = \frac{SS_E}{\mathrm{df_E}}. \tag{2.15b}$$

The expected values of the mean squares can be calculated as

$$E(MS_A) = \sigma^2 \frac{n}{I-1} \sum_i \alpha_i^2 \tag{2.16a}$$

$$E(MS_E) = \sigma^2. \tag{2.16b}$$

The expected values imply that inspecting the ratio between them would give good evidence against null hypothesis. Therefore the ratio $F = {}^{MS_A}/_{MS_E}$ is defined as test statistic, and the probability of obtaining a certain value for F under the null hypothesis, $P(F \mid H_0)$, is the output of the ANOVA test. Some hypothetical examples of how to interpret results of the ANOVA tests are shown in Table 2.2.

Chapter 3

Experiments

In this chapter the test equipment used is reported, together with test setup for all tests included in thesis.

3.1 Test Equipment

Cell tester Neware BTS-4000 All of the life cycle testing was performed on these cyclers. They are designed specifically for testing of cylindrical LIB cells with built-in cell holders. It has a voltage range up to 5 V and maximum current of 6 A, corresponding to a c-rate of about 1.33C for the cells tested in this study. It has a maximum sampling frequency of 10 Hz.

Potentiostat GAMRY Reference 3000 For electrochemical impedance spectroscopy a separate high accuracy potentiostat was used. The voltage range is up to 15 V with a maximum current of 3 A. The frequency range of EIS testing is 10 µHz to 1 MHz.

3.2 Test Object

All studies reported in thesis utilise the same test object, namely a 2170 Panasonic cylindrical cell from Tesla model 3. An overview of the specifications of the cell are listed in Table 3.1 and scanning electron microscopy images of the cross-section of the electrodes are shown in Fig. 3.1. It is an energy optimised cell intended for use between 2.55 V and 4.18 V, with a capacity of 4.6 A h for a weight of 68.45 g yielding an energy density of 242 W h kg^{-1}. At such high energy densities the risk of Li plating is typically higher compared to a more power optimised cell, therefore all charging is performed with a moderate C/3 current to avoid skewing results due to substantial Li plating.

Table 3.1: Technical specifications of the Panasonic 2170 cell.

Parameter	**Cell specifications**
Manufacturer	Panasonic
Geometry	Cylindrical 2170
Chemistry	NCA/Si-Gr
Capacity	4.6 A h
Weight	68.45 g
Height	70 mm
Diameter	21 mm
U_{max}	4.18 V
U_{min}	2.55 V
U_{nom}	3.6 V
Gravimetric energy density	242 W h kg^{-1}

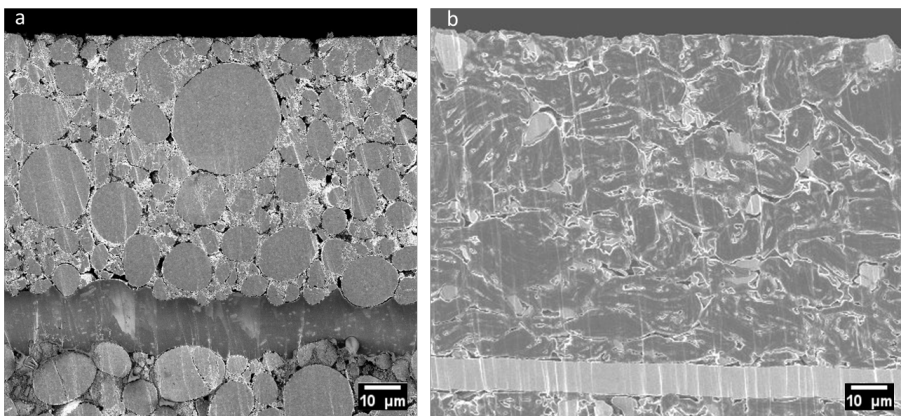

Figure 3.1: SEM of cross section of (a) positive NCA electrode and (b) negative SiO_x electrode. The metallic current collectors visible in lower part of images, the active material particles of various sizes and shapes above. Reproduced from **Paper III** under CC BY NC ND 4.0 license.

3.3 Reference Performance Test (RPT)

During cycling, regular checkups are performed to provide further detail into how the cells are ageing. The frequency of checkups vary between the studies, due to difference in the expected degradation [15], but it is always based on full cycle equivalent (FCE), which is chosen to make direct comparisons between the full and partial SOC window cycling possible. It converts partial cycling to full cycling by SOC window scaling, for example 10 cycles of 10%ΔSOC corresponds to 1 FCE.

The reference performance tests (RPTs) in all ageing tests performed in this project were performed following the same logic, as shown schematically in Fig. 3.2. The capacity test is performed by constant current, constant voltage (CCCV) charging with an initial current of C/3 and a cut-off current of C/20 at U_{max}, followed by a constant current (CC) discharge with C/3 to U_{min}. This test was designed to achieve accurate capacity measurements, which is the reason why capacity measurement is repeated twice and an average of the two measurements reported as capacity value for the corresponding RPT.

Moreover is should provide data for electrochemical analysis, partly by tracing the impedance through the pulse test, but mainly by doing a full CC C/20 charge and discharge cycle between U_{min} and U_{max} for ICA/DVA purposes, see Section 2.4.1 and Section 2.4.2 for details. After the ICA test the final part of the RPT is comprised of charge and discharge pulses at three SOC levels. To obtain comparable SOC levels throughout the cycling, the cell is first fully charged by CCCV C/3 with cut-off current C/20 to U_{max}. After this the cell is discharged by CC C/3 current to a voltage level corresponding to 70% SOC and a charge and discharge pulse at the maximum current of tester (6 A/1.33C) is performed. The discharge and pulsing is then repeated for 50% and 30% SOC as well.

3.4 Electrochemical Impedance Spectroscopy

To enable further electrochemical characterisation, a subset of the cells performed recurring EIS sweeps. The impedance sweeps were performed between 1 kHz and 10 mHz with high accuracy setting to reduce impact of noise on the EIS results.

3.5 Experimental Studies

The test matrices for the different substudies were designed to investigate ageing as a function of SOC and temperature, and of discharge frequency in the two main studies included in the thesis. The test conditions used are summarised in Table 3.2. The ΔSOC study was split into two studies with the results from "Small ΔSOC study" presented together with "Storage study" in **Paper II** and "Large ΔSOC study" presented in **Paper III**.

Table 3.2: Summary of all ageing tests performed in study. All cells were charged with C/3 current and discharged with an average current of 1C.

	Cells	T, °C	f, mHz	Min SOC	Max SOC	RPT	Test tag
Frequency study	2	25	1000	0	100	50 FCE	1000 mHz
	4	25	500	0	100	50 FCE	500 mHz
	4	25	250	0	100	50 FCE	250 mHz
	2	25	125	0	100	50 FCE	125 mHz
	4	25	62.5	0	100	50 FCE	62 mHz
	2	25	31.3	0	100	50 FCE	31 mHz
	4	25	15.6	0	100	50 FCE	16 mHz
	2	25	7.8	0	100	50 FCE	8 mHz
	3	25	3.9	0	100	50 FCE	4 mHz
1C reference	3	25	N/A	0	100	50 FCE	
Large ΔSOC study	2	25	N/A	0	100	50 FCE	R0-100
	2	25	N/A	50	100	50 FCE	R50-100
	2	25	N/A	0	50	50 FCE	R0-50
	2	45	N/A	0	100	50 FCE	H0-100
	2	45	N/A	50	100	50 FCE	H50-100
	2	45	N/A	0	50	50 FCE	H0-50
Small ΔSOC study	2	25	N/A	5	15	150 FCE	5-15% SOC
	2	25	N/A	15	25	150 FCE	15-25% SOC
	2	25	N/A	25	35	150 FCE	25-35% SOC
	2	25	N/A	35	45	150 FCE	35-45% SOC
	2	25	N/A	45	55	150 FCE	45-55% SOC
	2	25	N/A	55	65	150 FCE	55-65% SOC
	2	25	N/A	65	75	150 FCE	65-75% SOC
	2	25	N/A	75	85	150 FCE	75-85% SOC
	2	25	N/A	85	95	150 FCE	85-95% SOC
Storage study	2	25	N/A	15	15	Monthly	15% SOC
	2	25	N/A	50	50	Monthly	50% SOC
	2	25	N/A	85	85	Monthly	85% SOC

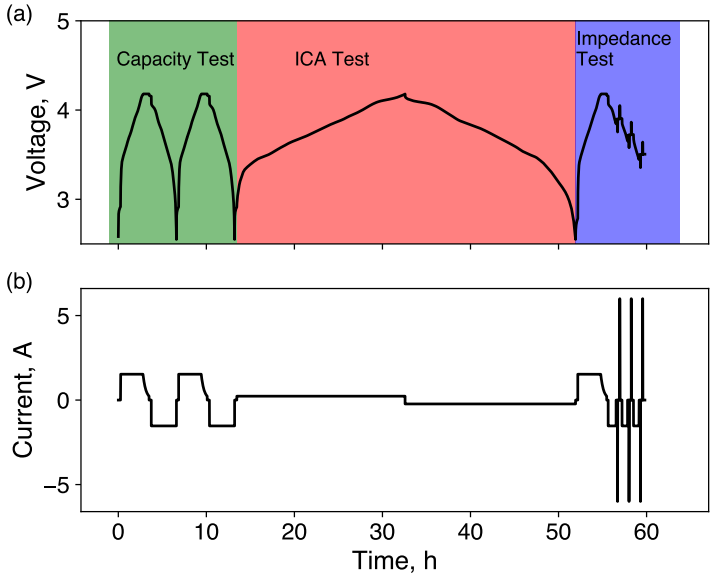

Figure 3.2: The RPT sequence used for regular checkups during ageing tests, (a) showing voltage profile, and (b) showing current profile.

3.5.1 Frequency Study

In the frequency study, reported in detail in **Paper I**, the influence of the discharge current pattern is investigated by altering the duration of the discharge and the rest part of a square wave discharge pattern, see Table 3.3, while maintaining an average discharge current of 1C which enables direct comparison with a standard 1C reference test. All other parameters, namely charge current, temperature and SOC window are kept constant to isolate the influence of the low frequency current dynamics.

The frequencies tested in the study were designed to obtain a suitable distribution in the frequency domain and seeking to complement previous studies which had focused on the high frequency domain [60]. The total time is varied according to $t_{total} = 2^N$ s with $N \in \{0, 1, \ldots, 8\}$ and the frequency defined as $f = {}^1/_{t_{total}}$.

All cells are tested using the built-in cylindrical cell holder of the Neware BTS-4000 tester, which uses a 4-wire connection for voltage and current measurements. For a subset of the cells there were EIS measurements performed every 300 cycles. These tests were run on a separate device as they require higher frequencies than 10 Hz that is the maximum sampling frequency of the cycler. This procedure therefore introduced shorter breaks in the cycling. To minimise the difference in the cycling conditions all cells were stopped during these periods and restarted at the same time.

Table 3.3: Schematic of pulse discharge pattern, where t_{total} refers to total pulse time, with two specific examples where $t_{total} = 2$ and 256 s respectively.

Discharge mode	**Time**	**Current**
Generic	0 - $^1/_4 t_{total}$	0C
	$^1/_4 t_{total}$ - t_{total}	1.33 C
	t_{total} - $^5/_4 t_{total}$	0C
	$^5/_4 t_{total}$ - $2t_{total}$	1.33 C
	⋮	⋮
2 seconds	0 - 0.5 s	0C
	0.5 - 2 s	1.33 C
	2 - 2.5 s	0 C
	2.5 - 4 s	1.33 C
	⋮	⋮
256 seconds	0 - 64 s	0C
	64 - 256 s	1.33 C
	256 - 320 s	0 C
	320 - 512 s	1.33 C
	⋮	⋮

Table 3.4: Voltage cut off limits used to define SOC windows in tests.

SOC, %	U_{low}	U_{high}
5-15	2.91 V	3.51 V
15-25	3.18 V	3.59 V
25-35	3.32 V	3.68 V
35-45	3.39 V	3.74 V
45-55	3.48 V	3.83 V
55-65	3.58 V	3.91 V
65-75	3.68 V	3.98 V
75-85	3.75 V	4.06 V
85-95	3.83 V	4.15 V

3.5.2 Small ΔSOC Study

In the small ΔSOC study the focus is to investigate the influence of the SOC window on the degradation in cells with mixed negative electrode materials. To achieve this a test matrix was designed with nine consecutive SOC windows defined by voltage cut-offs to avoid drifting in SOC during cycling. The SOC windows used and the corresponding voltage levels are detailed in Table 3.4. All cells were tested with a standard 1C discharge current and C/3 charge current. As the degradation is typically slower in partial SOC windows [15], [16] RPTs were performed less frequently, only every 150 FCE.

This study also entailed a set of calendar ageing tests. These were performed by charging the cells to a specific SOC and then leaving them without any load. After every 30 days an RPT was performed on the cells, with the addition of a full discharge and a CCCV charge to relevant SOC. Tests were performed at 15, 50 and 85% SOC.

3.5.3 Large ΔSOC Study

Similarly to the small ΔSOC study the large ΔSOC study focuses on elucidating the influence on ageing from different SOC windows, here in combination with temperature effects. This study therefore included three different SOC windows in combination with testing in two temperatures.

Furthermore, the study, in collaboration with partners at Uppsala University and Royal Institute of Technology, more heavily emphasised post-mortem investigation to confirm and extend the findings from the in-situ characterisation. This involved opening several cells in an Ar-filled glovebox to extract samples from both pristine and aged cells and for the positive as well as the negative electrode. These were then investigated using a range of experimental techniques

including inductively coupled plasma - optical emission spectroscopy (ICP-OES), X-ray diffraction (XRD), energy-dispersive X-ray spectroscopy (EDS) and SEM/transmission electron microscopy (TEM). For details on the post-mortem techniques the interested reader is referred to **Paper III**.

Chapter 4

Results Extracted from Appended Papers

This chapter summarises the results obtained from the three studies described in Chapter 3 investigating how discharge current frequency and SOC windows affect battery degradation.

4.1 Effect of Dynamics in Cycling

The cycling of cells were conducted during 2020 and 2021, with initial results indicating surprisingly large spread in data between replicates. This prompted the addition of further tests in the instances where large spread was seen. This led to somewhat uneven distribution in number of cells tested, which can be seen from Table 3.2. The results presented below include all of the tested cells as no errors in test conditions could be found, so the spread is assumed to be a consequence of cell quality and should be taken into consideration for the study.

The summarised degradation data for all the cells cycled with different discharge frequencies are presented in Fig. 4.1. As mentioned above, already from this figure a significant spread can be noted for the replicates, which makes analysis based directly on inspecting the capacity fade versus FCE difficult. However a weak trend can be noted, namely that the cells discharging with a lower frequency age at a slower rate compared to those at higher frequencies.

To clarify the results, another metric is introduced where the energy throughput at end of life (EOL), defined as 75% of initial cell capacity, is calculated. This yields a single data-point per replicate which after grouping by frequency can be plotted as a box plot with the average and the spread for each set of replicates, see Fig. 4.2. From this plot the trend is more clearly visible with a tendency for the energy throughput to decrease with increasing frequency. This trend is however stronger in lower frequency ($f < 100\,\mathrm{mHz}$), and when only inspecting higher frequency no clear trend can be seen.

The surprisingly large spread between replicates still makes it hard to discern

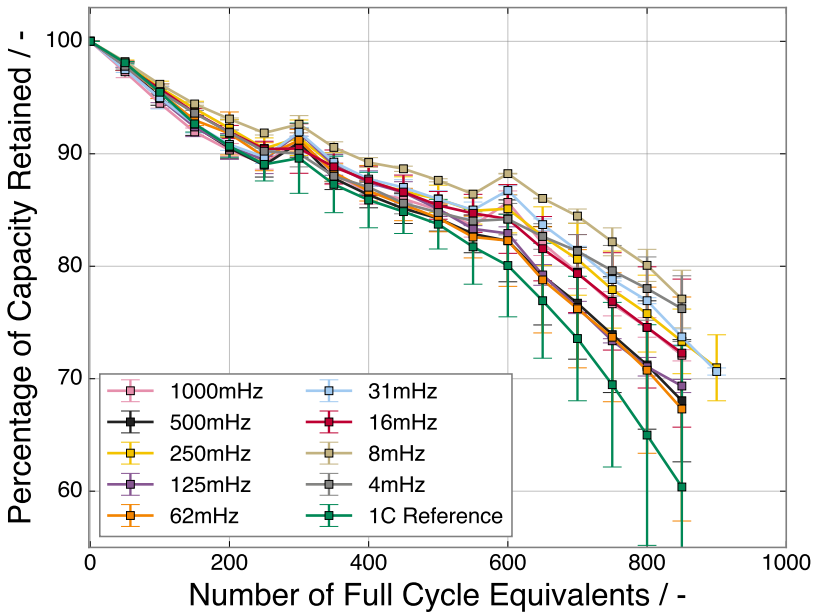

Figure 4.1: Capacity fade of all cells tested in the frequency study, together with the 1C reference. Worth noting significant spread in results between replicates. See Table 3.2 for test conditions.

between noise and trend, so to be able to draw any conclusions statistical analysis is required. For this dataset, the ANOVA test is appropriate, as it is designed to check the null hypothesis of background noise versus an actual existing trend. In this work the ANOVA test is used and implemented in the R software [61]. That is, it seeks to investigate if the variations in the results can be explained by natural variance, or if that null hypothesis can be rejected, see Section 2.5 for further details.

The null hypothesis, H_0, being that the actual means are the same for all data in the set, and any apparent differences are only due to the variance of the data. To assess whether the null hypothesis can be rejected the probability $P(H_0)$ is calculated for a given dataset. In this study $P(H_0) < 0.05$ is set as significance condition for rejecting the null hypothesis.

As a first step $P(H_0)$ is calculated for the full dataset resulting in $P(H_0) = 0.28$, or that there is a 72% probability that we can reject null hypothesis. Since this is above the significance threshold, the null hypothesis can not be rejected for the full set.

However, as was noticed earlier, the trend is not equal across the dataset, but seems to be stronger in the frequencies below 100 mHz. Therefore a split of the dataset is introduced to assess whether a statistically significant trend can be identified in the low frequency region. By performing the ANOVA analysis for only $f < 100\,\text{mHz}$ a probability of $P\left(H_0 \mid f < 100\,\text{mHz}\right) = 0.028$ is obtained, meaning that in the lower frequency domain a statistically significant trend exists, and the null hypothesis can be rejected with 97.2% probability.

On the high frequency part of the dataset on the other hand, the ANOVA test yields $P\left(H_0 \mid f > 100\,\text{mHz}\right) = 0.81$. This means that there is only a 19% probability that the null hypothesis can be rejected and no trend can be said to exist in this frequency range.

This strengthens the initial observation that there is a positive trend of cycle life when decreasing the cycling frequency, at least down to $\sim 4\,\text{mHz}$. However, the trend is not universal as all dynamic tests outperform the 1C reference case, which could be conceptualised as "zero" frequency by the convention of this study. This suggests that it could be of interest to further investigate ageing behaviour in the low frequency domain, preferably on a cell with less individual variance.

The trend that the high frequency cycling has little to no impact on the cycle life also fits well with the results found by Bessman, Soares, Wallmark *et al.* [60], who saw little influence when investigating $f > 1\,\text{Hz}$. One should however keep in mind that even though no trend exists within the $0.1\,\text{Hz} < f < 1\,\text{Hz}$ domain, all these tests significantly outperform the 1C reference, so to realistically assess the cycle life of cells for a commercial application for instance, testing of dynamic cycling in this frequency range is definitely relevant.

4.2 Effect of Low SOC Cycling

The study of different SOC windows was conducted in parallel with the frequency study and using the same Panasonic 2170 cell as test object. Further

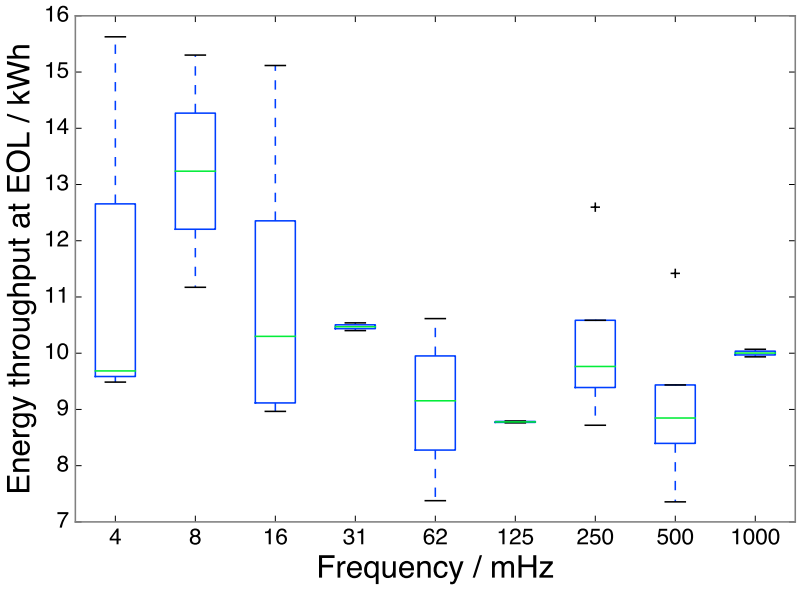

Figure 4.2: Distribution of the energy throughput at EOL for cells cycled at different frequencies. Large spread is visible in numerous samples. Note that this does not include the 1C reference. Reproduced and adapted from **Paper I**.

information about the cell can be found in Table 3.1. In this study comparatively less heterogeneity was found between samples, meaning that it was sufficient for all tests to be performed with 2 replicates, see Table 3.2 for further test condition information. For the smaller ΔSOC windows all tests were conducted at the same temperature, and for the large ΔSOC windows every test was performed in two temperatures, at 25 °C and 45 °C. The naming convention used for all figure legends reflect SOC window for small ΔSOC windows and temperature and SOC window for large ΔSOC windows.

All the data from the cycling study is summarised in Figures 4.3 and 4.4. From the data the overall trend that low SOC cycling has a detrimental effect on the capacity retention is clear. Worth noting in particular is that 5-15% and 15-25%SOC tests stand out with especially rapid degradation in the small ΔSOC study. This trend is more pronounced in the early stages of ageing with the capacity decay levelling out after approximately 1000 FCE, whereas for the large ΔSOC study the trend is continuous for all tests that cycle to low SOC. The dominance of the influence of low SOC windows on ageing can also be demonstrated by noting that all cases in large ΔSOC study that cycle to low SOC are closely grouped. As seen from Fig. 4.3 this happens regardless of the maximum SOC and the temperature. Ont he other hand, the tests that cycle with higher miniumm SOC, that is $SOC_{min} = 50$, show a clear temperature

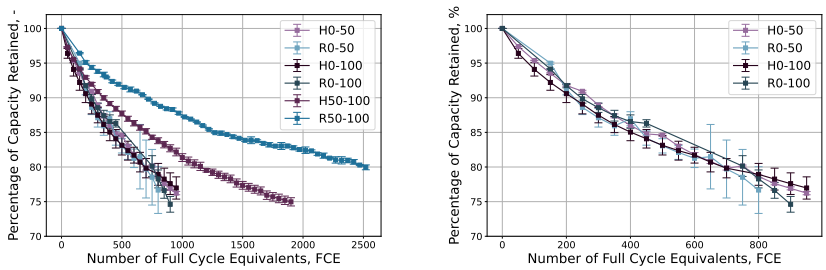

(a) (b)

Figure 4.3: Capacity fade cells tested in large SOC windows. All cells shown in (a) with a subset of cells cycled to 0% SOC shown in (b) to improve visibility. Legends are consistent with test tag in Table 3.2. Reproduced from **Paper III**.

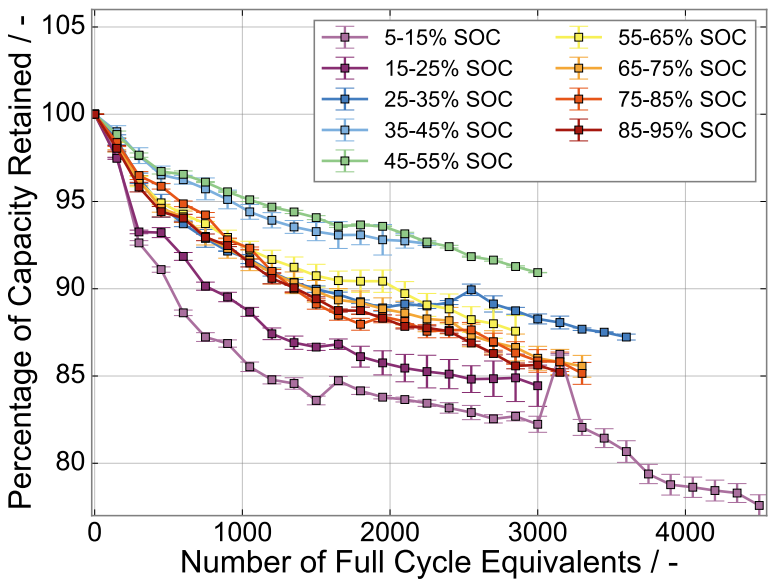

Figure 4.4: Capacity fade of cells tested in small ΔSOC windows. Legends are consistent with test tag in Table 3.2. Reproduced and adapted from **Paper II**

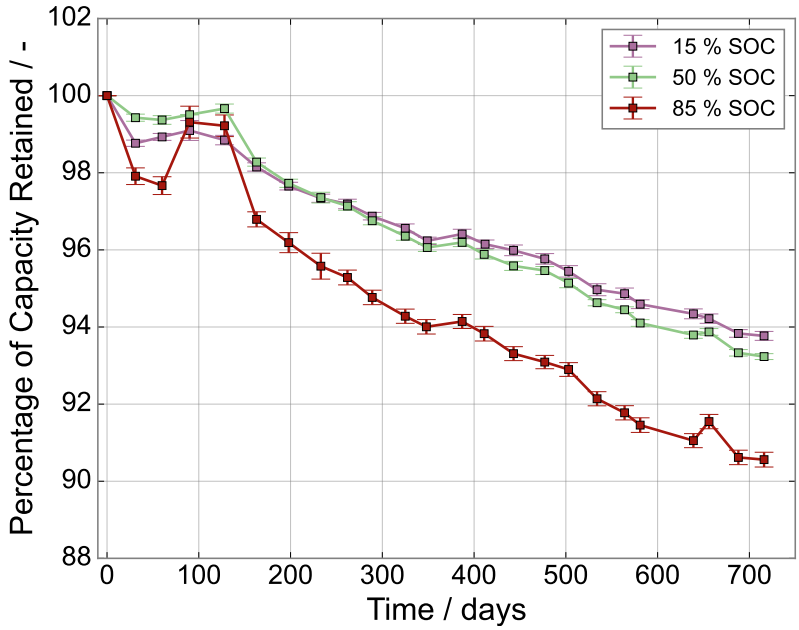

Figure 4.5: Capacity retention of calendar tested cells. Reproduced and adapted from **Paper II**.

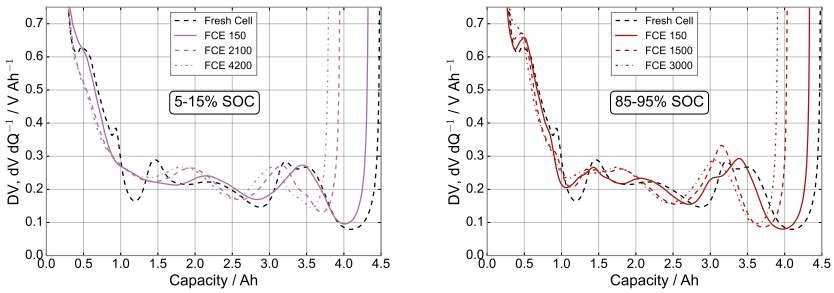

(a) (b)

Figure 4.6: Comparison of DVA development with ageing for 5-15% case, shown in (a), and 85-95% case, shown in (b). The effect of low SOC cycling is clearly visible in loss of SiO_x related peaks in low SOC for 5-15% case. Reproduced and adapted from **Paper II**.

dependence, where a lower temperature reduces the rate of degradation.

The reason behind this strong SOC dependence can be investigated with in-situ techniques, especially utilising DVA and tracking peaks corresponding to each material in the electrodes. In Fig. 4.6 a comparison of DVA profiles for 5-15% SOC, Fig. 4.6(a), and 85-95% SOC, Fig. 4.6(b), is shown. For 5-15%, already at 150 FCE peaks S1 and S2 (see Fig. 2.6 for peak assignment), which are characteristic for SiO_x, are nearly lost. However in the 85-95% case S1 and S2 are still well-defined after 150 FCE. As cycling proceeds the SiO_x are completely lost in the low SOC case and the DVA profile is losing features overall, except for the NCA peaks. This is indicative of inhomogeneous ageing in the electrode which leads to multiple lithiation stages coexisting in different locations in the cell leading to smearing out of equilibrium potentials.

Also visible from Figures 4.6(a) and 4.6(b) is the overall shift of the peaks leftward which can be seen as further indication that SiO_x, which contributes to the capacity in low SOC, is being lost. It can also be indicative of loss of lithium inventory (LLI), which is investigated in greater detail using DVA peak tracking, see below.

The decrease in active SiO_x can be further corroborated by analysis of the voltage hysteresis, ie the difference in voltage for the same SOC during slow galvanostatic charge and discharge cycling, see Section 2.4.3. The hysteresis calculation for a C/20 cycle is visually represented in Fig. 4.7(a) with repeated hysteresis calculations during cycling shown for 5-15% in Fig. 4.7(b) and for 85-95% in Fig. 4.7(c) respectively. It shows a clear disparity in hysteresis in low SOC (approximately $< 15\%$) between the two cases. For the 5-15% cycling case, the hysteresis decreases from $\sim$250 mV at beginning of life (BOL) to approximately 200 mV after 1200 FCE. For the 85-95% case the decrease is significantly smaller with hysteresis only decreasing to about 240 mV after 1200 FCE.

To extend this qualitative assessment of Gr-SiO_x ageing, DVA was utilised to

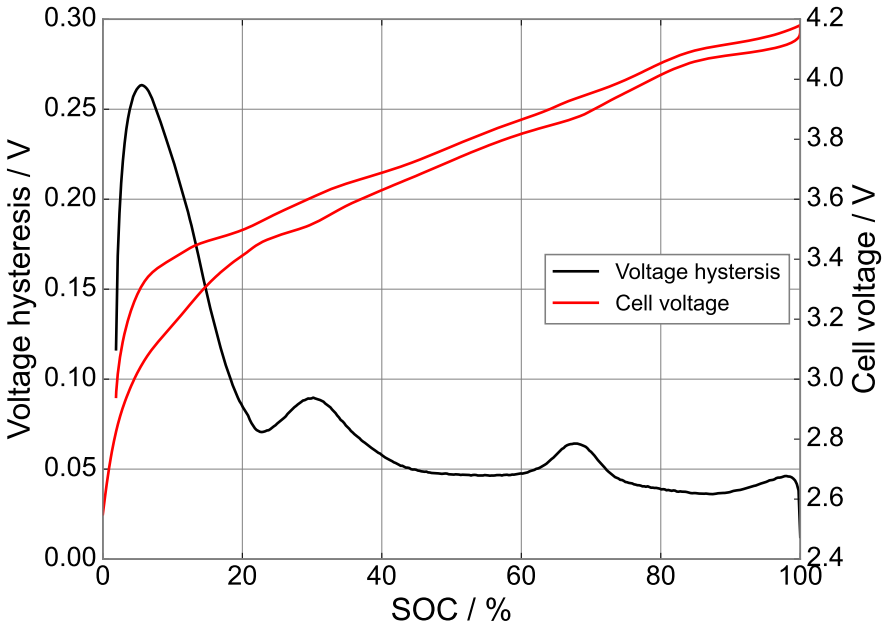

(a)

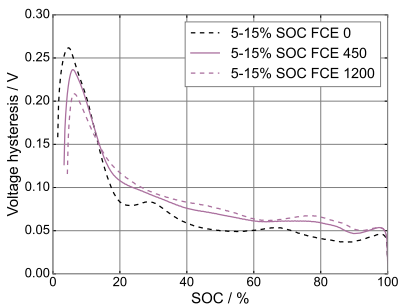

(b)

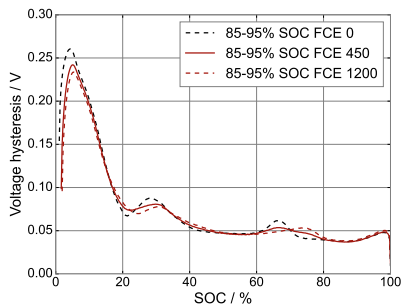

(c)

Figure 4.7: Comparison of the voltage difference between the charge and discharge part at the same SOC during C/20 cycling for (a) a full cell at BOL, (b) a cell cycled in 5-15% SOC window at three ageing stages, and (c) a cell cycled in 85-95% SOC window at different stages of ageing. Reproduced and adapted from **Paper II**.

make quantitative analysis of ageing modes to further elucidate the degradation processes in the cells. This was done following a method detailed by Smith, Svens, Varini *et al.* [in 62] where by tracking the DVA peak distances during cycling, the overall capacity fade can be attributed to loss of active material on each material as well as loss of lithium inventory. The results from DVA peak tracking are presented in Fig. 4.8 where Fig. 4.8(a) and (b) display all DVA curves with artifical offset, and 4.8(c) and (d) show the corresponding LAM and LLI trackers. Though the heterogeneity and resulting smearing/convolution of peaks caused some numerical issues and made the results somewhat jumpy, it still allows for concluding that $\mathrm{LAM}_{\mathrm{SiO}_x}$ contributes to ageing in a low SOC cycling to a significantly larger extent than in high SOC cycling. In the 5-15% case it contributes 7% of overall ageing compared to 3% in 85-95% case. Also noteworthy is that the bulk of $\mathrm{LAM}_{\mathrm{SiO}_x}$ happens in the first $\sim$1000 FCE and flattens out for the rest of cycling, see Fig. 4.8(c). This corresponds well with the overall capacity loss which show a more rapid capacity decay in the first $\sim$1000 FCE to flatten out at a later stage, see Fig. 4.4, which indicates that degradation due to $\mathrm{LAM}_{\mathrm{SiO}_x}$ contributes disproportionately to ageing until a significant portion of SiO_x is lost.

For both the tests investigated with DVA peak tracking, the main loss factor can be concluded to be LLI, see Figures 4.8(c) and (d). The LLI is particularly dominant for the 5-15% SOC cycling. Through post-mortem work performed at Uppsala University and described in detail in **Paper III** this is shown to be heavily influenced by the formation and reformation of dendritic SEI on SiO_x particles, which consumes Li^+ . Post-mortem analysis also revealed pore development in SiO_x particles that could also contribute to trapping of Li , and cause electrical isolation that leads to LAM.

For tests performed at high SOC the increase in capacity loss is attributed to $\mathrm{LAM}_{\mathrm{NCA}}$ in the post-mortem investigation. In particular the findings show that particle fractures lead to voids in positive electrode particles and irreversible capacity loss.

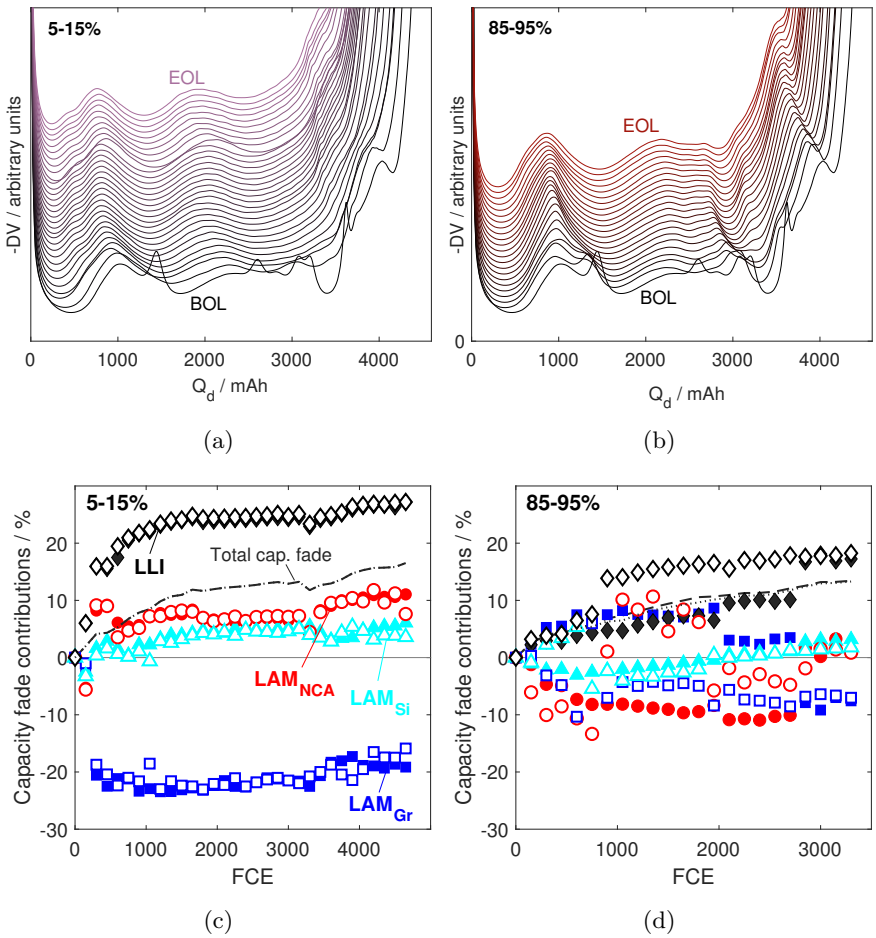

Figure 4.8: DVA from all RPT through cycling shown for (a) 5-15% SOC cycling, and (b) 85-95% SOC window. (c) and (d) display key ageing factors tracked for each DVA during cycling. Reproduced from **Paper II**.

Chapter 5

Charge Current Pulsing

The results and hypotheses presented in this chapter are unpublished as of yet. Therefore the status is still that of work-in-progress, but the most interesting parts are still included in this thesis as an example of the ongoing and upcoming work in the project.

From the findings of the Frequency study a couple of new questions arose that is to be addressed in coming works. Given that the focus in the previous study was entirely on discharge profiles the question arose whether the same type of influence would be present for charge current patterns, with specific interest in how it could affect Li plating.

To further analyse the internal processes, the decision was made to couple the experimental cycling with electrochemical modelling, so in order to enable this, the well researched 18650 LG MJ1 cell was chosen, for which a full electrochemical parameter set has been published by Sturm, Rheinfeld, Zilberman *et al.* [see 63], which can be seen in Table 5.1. The cell is highly energy optimised with a nominal capacity of 3.5 A h with a gravimetric energy density of 260 W h kg^{-1} referenced to a cell weight of 49 g and nominal voltage of 3.64 V.

The pulse charging was defined as a combination of a 1C square wave with a 50% duty cycle and a duration of t_{tot} superpositioned with a DC current of 1C. This yields an average current of 1C and is visualised in Fig. 5.1. Similarly to the frequency study, the frequency is defined as $f = {}^{1}/_{t_{tot}}$ and a total of seven different frequencies are tested spanning from 10 mHz to 100 Hz. The same current pattern were utilised for both the charge and discharge cycling.

The capacity fade of the tested cells are shown in Fig. 5.2. There is a clear grouping of the tested cells where all cells cycled with a frequency below $f = 1$ Hz degrading significantly faster than the cells cycled at higher frequency. This interestingly is contrary to the findings in the frequency study presented in Section 4.1. With consideration to that both cycle pattern and cell is different to that study, it is still an indication that other degradation processes are triggered when pulsing both charge and discharge compared to pulsing only the discharge current. It is also clear that cycle life at the tested current conditions is very limited with none of the cells reaching more than 300 cycles before

Table 5.1: Parameters used for physical model of LG MJ1 cell with NCM 811 ($LiNi_{0.8}Co_{0.1}Mn_{0.1}O_2$) positive electrode and mixed graphite-SiO_x negative electrode. Values as reported in [63].

Parameter	Positive electrode	Separator	Negative electrode
Thickness L	66.2 µm	12 µm	86.7 µm
Particle radius R_p	3.8 µm		6.1 µm
Porosity ϵ	17.1%	45%	21.6%
Additives	8.4%		9%
Bruggeman coefficient β	1.85	1.5	1.5
Maximum concentration $c_{s,\max}$	$50\,060\,\mathrm{mol\,m^{-3}}$		$34\,684\,\mathrm{mol\,m^{-3}}$
Solid state diffusivity D_s	$5 \times 10^{-13}\,\mathrm{m^2\,s^{-1}}$		$5 \times 10^{-14}\,\mathrm{m^2\,s^{-1}}$
Conductivity σ_s	$0.17\,\mathrm{S\,m^{-1}}$		$100\,\mathrm{S\,m^{-1}}$
Rate constant k_{ct}	$1 \times 10^{-11}\,\mathrm{m\,s^{-1}}$		$3 \times 10^{-11}\,\mathrm{m\,s^{-1}}$
Transfer coefficient α	0.5		0.5
	Electrolyte (1 M $LiPF_6$ in PC/EC/DMC)		
$LiPF_6$ Diffusivity D_l	$10 \times 10^{-4}\,\mathrm{m^2\,s^{-1}}$		
Transference t_+^0	0.38		
Ionic conductivity σ_l	$0.1\,\mathrm{S\,m^{-1}}$		
Reference concentration c_{ref}	$1000\,\mathrm{mol\,m^{-3}}$		

dropping below 80% capacity retention.

In order to investigate the reason for these very distinct ageing patterns for different groups of frequencies, the same current pattern was simulated. This is to be able to get explicit values for battery internal parameters that can not be measured from testing of full cells. Though the accuracy of the model is not perfect, the results should give an indication of certain critical parameter values and thus help determine which ageing phenomena is triggered. As the cells degrade at a very rapid pace during the cycling, one possible theory is that Li plating could be a main contributor to degradation. Therefore specific focus is directed towards the charging part of the cycling. The model was implemented in COMSOL Multiphysics using the Batteries and Fuel Cells interface, with physical parameters as listed in Table 5.1. To reduce computational effort the simulations were broken up into smaller sections where relevant processes could be studied. The case reported in this study is charging from 80% SOC, chosen to study potential onset of Li plating while avoiding numerically expensive voltage adaptation due to max voltage being reached on full cell.

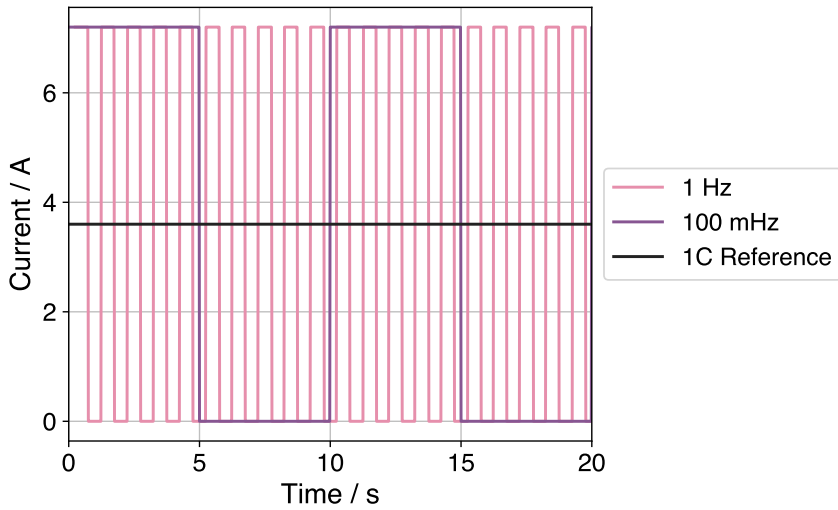

Figure 5.1: Schematic representation of charge profiles for 1 Hz, 100 mHz and 1C reference.

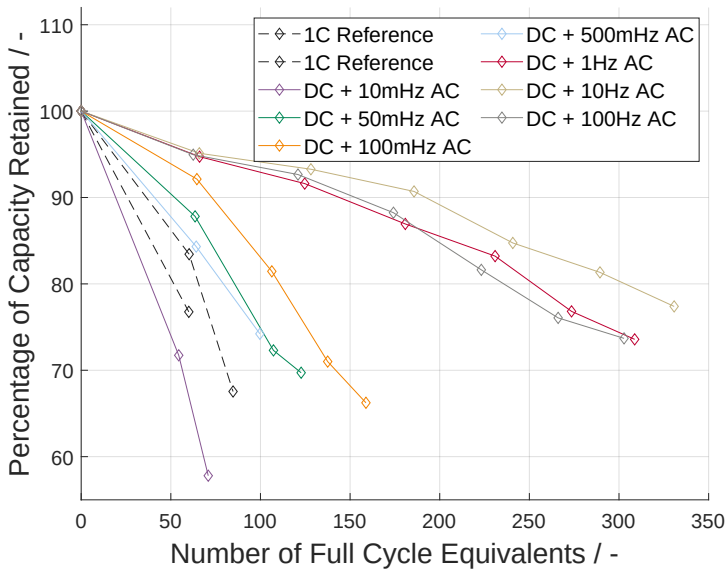

Figure 5.2: Capacity fade for all tested frequencies and 1C reference.

Recalling the conditions in which Li plating can occur, see Section 2.3.2, the main conditions to investigate would be Li saturation on the surface of particles, most likely to commence near the separator, and the overpotential of the kinetic Li plating reaction. As the formation of Li on the surface of the electrode is a reduction process, it is triggered when overpotential drops below zero, $\eta < 0$. The results of the simulation for these two parameters are shown in Fig. 5.3, with a subset of frequency test chosen for visibility, two examples of lower frequency (50 and 100 mHz) with fast degradation and one case with higher frequency (1 Hz) and less rapid ageing. By recalling that the maximum concentration of the negative electrode is $34\,684\,\mathrm{mol\,m^{-3}}$ it can quickly be concluded from Fig. 5.3(a), where maximum concentrations reach around $27\,000\,\mathrm{mol\,m^{-3}}$, that there is sufficient margin to saturation concentration of the material. The margin is large enough that even the localised effects, that have been disregarded for simplicity and run time in the pseudo-two-dimensional (P2D) model, would likely not lead to locally exceeding the maximum concentration. From Fig. 5.3(b) it is however clear that kinetic Li plating could be triggered for all cases of cycling, already from the moderate 80% SOC where simulation initiates. Although the lower frequency cases reach negative overpotentials of somewhat larger magnitude than the higher frequency case, the overpotential still drops well below 0 V *vs.* $\mathrm{Li/Li^+}$ also for 1 Hz cycling.

Based on these observations, established Li plating models which have no time dependence, see Section 2.3.2.1, would offer no clear explanation as to why there would be a clear degradation threshold between 0.5 Hz and 1 Hz. The results could indicate that there is a duration required to trigger the onset of Li plating, but from the available data it is not possible to discern whether this would be due to plating underpotentials, mass transfer limitations or some other phenomenon that could hinder the onset of Li plating.

This is however an interesting topic to investigate further as understanding the frequency dependence of Li plating could help increase fast charging while avoiding the most severe bi-product, which is Li plating. As these results are still preliminary and have not yet been published, further investigation of this topic through both extended experimental and computational efforts will be an important focus during the remainder of this project.

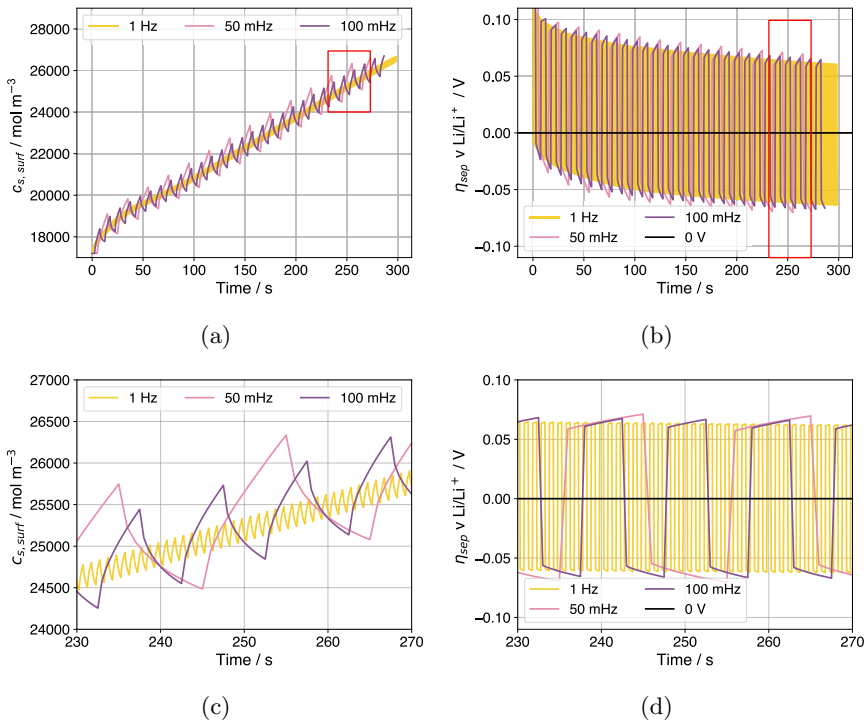

Figure 5.3: Simulation results for two common triggers of Li plating for the cases of 0.05, 0.1 and 1 Hz. In (a) the concentration of Li on the particle surface of the negative electrode near separator is shown for full simulation duration, and (b) shows the Li plating reaction overpotential, η, near the separator during full simulation. In (c) and (d) a magnified version of (a) and (b) respectively are shown for visibility. The zoomed in area is indicated by red frame.

Chapter 6

Conclusions

In this thesis test matrices including comprehensive testing for SOC dependence and discharge current pulse frequency dependence is presented. From the data it can be concluded that it is important to take dynamic usage into account when investigating the ageing behaviour of LIBs, especially in the lower frequency range ($\sim f < 100$ to 500 mHz). A strong SOC dependence was shown with the capacity loss being most rapid in low SOC (<25%), slowest in mid SOC range, with an acceleration in high SOC.

Cycling in smaller Δ SOC windows degrade the tested cells slower compared to larger Δ SOC windows, which is in line with previously reported results [15]. The study could also confirm previous studies with regards to temperature effect with lower temperatures reducing the degradation rate. The SOC influence was however dominant, especially in low SOC cycling, demonstrating that influence of temperature on cycling ageing is weaker compared to SOC dependence for cells with mixed negative electrodes containing SiO_x.

The rapid degradation in low SOC could also be attributed to the influence of SiO_x, both in contribution to LLI due to formation of unstable SEI and due to LAM_{SiO_x} during cycling. The increase in degradation in high SOC windows could be attributed to increasing LAM_{NCA}.

In work currently ongoing, a strong influence on frequency for pulsed charged currents was found. The degradation is grouped with cells pulse charging where $f < 1$ Hz ageing more rapidly than cells charged with higher pulse current frequencies. Through simulations, a hypothesis is formulated that this could possibly be attributed to Li plating, indicating a threshold duration for onset of Li plating.

Chapter 7

Future Work

The results up to now have raised many interesting questions which can be followed up by future work. Some of it is in fact already ongoing or being planned.

The large spread in degradation performance between replicates of the same test raises several questions that can be investigated. For instance the causes of heterogeneity in ageing can be further researched through more detailed post-mortem analysis of multiple replicates from the same ageing test procedure. Another interesting approach would be to investigate the impact that the variability has on the requirements for ageing test matrices, and the possibility to draw conclusions from limited data sets. This would require tests with more replicates to be able to confidently assess variance between samples, and could provide important input to design of experiments for future studies.

The possibility to use physical models for both elucidating internal processes in the battery during cycling as well as explicitly model the side reactions would offer interesting opportunities for further studies and more accurate physical modelling. Implementation of explicit Li plating models for the cell studied in the pulse charge study is currently being planned, and modelling of further commercial cells being investigated. Further studies that would be interesting is to investigate the modelling of coupling between Li plating and SEI growth, which could be done by augmenting the Li plating model equations with a correlation to potential drop due to SEI film growth.

Further study of the influence of pulsed charge current, involving other cells, more replicates, and investigation of SOC dependency would provide interesting insights applicable to design of fast charging protocols. This would also provide further input to understanding of for instance Li plating, and give further opportunities to investigate a possible dependence on duration of negative overpotential.

Chapter 8

Summary of Included Papers

8.1 Low Frequency Influence on Degradation of Commercial Li Ion Battery

In this paper we present the influence of low frequency (<1 Hz) current harmonics on ageing in a commercial LIB.

Problem

Electric vehicle usage of batteries is very different to the more idealised utilisation in laboratory studies of ageing, which typically utilise constant current charge and discharge to scope the degradation of battery cells. In this paper we seek to introduce an alternative testing methodology with parameterisable discharge patterns to closer emulate usage in a real application while maintaining governing parameters to a manageable set.

Contribution

In this paper we introduce a testing method for parametrisable dynamic battery testing, which makes it possible to elucidate the influence of low frequency current harmonics on battery degradation using a standard battery tester. The focus in this paper is on discharge current harmonics, but could be implemented analogously for charge currents, or combinations of both.

The cycling resulted in statistically significant influence on ageing from current frequency in the region below $f < 0.1\,\text{Hz}$, but no influence could be found in region where $f > 0.1\,\text{Hz}$. Furthermore a clear preference for dynamic cycles over the reference constant current 1C cycle which performed significantly worse than all tested pulse frequencies (0.04 Hz to 1 Hz).

Methodology

The test protocol is a square wave profile with average discharge current the same as a standard 1C discharge. This was implemented on a standard NEWARE BTS-4000 battery cycler with regular checkup tests performed every 50 Full cycles. In every checkup capacity, impedance and incremental capacity measurements were performed to assess the battery degradation.

8.2 The state of charge dependence of degradation in lithium-ion cells from a Tesla model 3

In this paper we present an ageing study of NCA positive electrode and mixed graphite/SiO_x negative electrode commercial cells with the focus on the SOC dependence of ageing.

Problem

Findings from literature indicate that there is a correlation between SOC and both cycling and storage ageing of LIBs. The nature of the correlation is however highly dependent on the battery chemistry and configuration. Elucidating this influence is important to take into account when designing battery control systems and usage strategies to maximise battery life.

Contribution

The capacity face results for cells with NCA positive electrode and mixed graphite/SiO_x negative electrode cycled in sequential 10% SOC windows are presented. Furthermore extensive in-situ analysis is performed to explain the processes behind ageing in different SOC windows with particular focus on low SOC region.

Furthermore calendar ageing results for three SOC levels (15%, 50% and 85%) are reported.

In this paper we show an unexpected SOC-ageing correlation where cells cycled in low SOC age more rapidly than those cycled in higher SOC, with an optimum found in the region of 35-75% SOC and slight increase in degradation above 75% SOC. For calendar tests the trend was the opposite with high SOC cells degrading faster than low SOC cells.

In the low SOC region it is found that SiO_x contribute disproportionately to the rapid degradation with a loss of cyclable SiO_x. This is concluded from ICA, DVA and hysteresis analysis, which also show that loss of lithium inventory (LLI) is the main contributor to loss of overall capacity in the cells cycled in low SOC.

Methodology

Nine consecutive 10% SOC windows were defined by voltage limits and cycling performed with 1C constant current discharge and C/3 charge. Regular checkups with capacity, impedance and incremental capacity measurements were performed every 150 cycles. Each test was run with duplicate cells to ensure reproducibility of results, yielding a total of 18 cycled cells and 6 calendar aged cells.

The main techniques utilised to understand ageing processes are ICA and DVA. Using ICA to demonstrate qualitatively the loss of active silicon and heterogeneity in ageing, and DVA to seek to quantify loss of silicon and also LLI.

8.3 Ageing of High Energy Density Automotive Li-ion Batteries: The Effect of Temperature and State-of-Charge

Similarly to **Paper II** we focus on the SOC influence on ageing in this paper. Here the focus is shifted to larger SOC windows and positive electrode degradation.

Problem

Understanding both the SOC and temperature influence on ageing in commercial EV cells is necessary to be able to develop optimise usage strategies for both drivers and manufacturers.

Contribution

In this paper we show that ageing on positive electrode due to TM dissolution happens at a higher rate in high SOC and high temperature conditions. Post-mortem analysis also confirmed that LLI is the main cause for overall capacity loss. It also confirmed that loss of silicon capacity is many times higher than loss of graphite capacity and therefore is the main contributor to capacity loss on negative electrode. With similar findings from in-situ electrochemical analysis as in **Paper II** the post-mortem results corroborate the results of the parallel study as well.

Methodology

Three different SOC windows (0-50%, 50-100% and 0-100%) are defined and cycling is performed in two temperatures (25 °C and 45 °C) for each of these SOC windows, with two duplicates performing each test, yielding a cycling test matrix of six tests and twelve cells.

Additionally extensive post-mortem analysis was performed on samples taken from cycled cells. This included electrochemical measurements (intermittent current interruption (ICI), ICA, EIS) as well as microscopy (SEM TEM), spectroscopy techniques (EDS and ICP-OES) and XRD.

Bibliography

[1] UN, "Fact sheet climate change," 2021, Sustainable Transport Conference, Beijing (cit. on p. 3).

[2] H. Ritchie, "Cars, planes, trains: Where do co2 emissions from transport come from?" *Our World in Data*, 2020, https://ourworldindata.org/co2-emissions-from-transport (cit. on p. 3).

[3] C. Simpson, E. Ataii, E. Kemp and Y. Zhang, "Mobility 2030: Transforming the mobility landscape," KPMG Global Strategy Group, Tech. Rep., 2019 (cit. on p. 3).

[4] A Ajanovic and R Haas, "Economic and environmental prospects for battery electric-and fuel cell vehicles: A review," *Fuel cells*, vol. 19, no. 5, pp. 515–529, 2019 (cit. on p. 3).

[5] M. Armand and J.-M. Tarascon, "Building better batteries," *nature*, vol. 451, no. 7179, pp. 652–657, 2008 (cit. on pp. 3, 8).

[6] M. Dubarry, C. Truchot and B. Y. Liaw, "Cell degradation in commercial lifepo4 cells with high-power and high-energy designs," *Journal of Power Sources*, vol. 258, pp. 408–419, 2014 (cit. on p. 4).

[7] D. Cui, J. Wang, A. Sun, H. Song and W. Wei, "Anomalously faster deterioration of lini0. 8co0. 15al0. 05o2/graphite high-energy 18650 cells at 1.5 c than 2.0 c," *Scanning*, vol. 2018, 2018 (cit. on p. 4).

[8] J. Li, J. Harlow, N. Stakheiko, N. Zhang, J. Paulsen and J. Dahn, "Dependence of cell failure on cut-off voltage ranges and observation of kinetic hindrance in lini0. 8co0. 15al0. 05o2," *Journal of The Electrochemical Society*, vol. 165, no. 11, A2682, 2018 (cit. on p. 4).

[9] Y. Gao, J. Jiang, C. Zhang, W. Zhang and Y. Jiang, "Aging mechanisms under different state-of-charge ranges and the multi-indicators system of state-of-health for lithium-ion battery with li (nimnco) o2 cathode," *Journal of Power Sources*, vol. 400, pp. 641–651, 2018 (cit. on p. 4).

[10] L. Tan, L. Zhang, Q. Sun, M. Shen, Q. Qu and H. Zheng, "Capacity loss induced by lithium deposition at graphite anode for lifepo4/graphite cell cycling at different temperatures," *Electrochimica Acta*, vol. 111, pp. 802–808, 2013 (cit. on p. 4).

[11] T. Waldmann, M. Kasper and M. Wohlfahrt-Mehrens, "Optimization of charging strategy by prevention of lithium deposition on anodes in high-energy lithium-ion batteries–electrochemical experiments," *Electrochimica Acta*, vol. 178, pp. 525–532, 2015 (cit. on p. 4).

[12] A. Friesen, X. Mönnighoff, M. Börner, J. Haetge, F. M. Schappacher and M. Winter, "Influence of temperature on the aging behavior of 18650-type lithium ion cells: A comprehensive approach combining electrochemical characterization and post-mortem analysis," *Journal of power sources*, vol. 342, pp. 88–97, 2017 (cit. on p. 4).

[13] Y. Preger, H. M. Barkholtz, A. Fresquez *et al.*, "Degradation of commercial lithium-ion cells as a function of chemistry and cycling conditions," *Journal of The Electrochemical Society*, vol. 167, no. 12, p. 120 532, 2020 (cit. on p. 4).

[14] J. de Hoog, J.-M. Timmermans, D. Ioan-Stroe *et al.*, "Combined cycling and calendar capacity fade modeling of a nickel-manganese-cobalt oxide cell with real-life profile validation," *Applied Energy*, vol. 200, pp. 47–61, 2017 (cit. on p. 4).

[15] E. Wikner, *Ageing in Commercial Li-ion Batteries: Lifetime Testing and Modelling for Electrified Vehicle Applications*. Chalmers University of Technology, 2019 (cit. on pp. 4, 23, 27, 45).

[16] P. Keil and A. Jossen, "Impact of Dynamic Driving Loads and Regenerative Braking on the Aging of Lithium-Ion Batteries in Electric Vehicles," *Journal of The Electrochemical Society*, vol. 164, no. 13, A3081–A3092, 2017, ISSN: 0013-4651. DOI: 10.1149/2.0801713jes (cit. on pp. 4, 27).

[17] G. Baure and M. Dubarry, "Synthetic vs. Real driving cycles: A comparison of electric vehicle battery degradation," *Batteries*, vol. 5, no. 2, p. 42, 2019, ISSN: 23130105. DOI: 10.3390/batteries5020042 (cit. on p. 4).

[18] A. J. Crawford, Q. Huang, M. C. Kintner-Meyer *et al.*, "Lifecycle comparison of selected li-ion battery chemistries under grid and electric vehicle duty cycle combinations," *Journal of Power Sources*, vol. 380, pp. 185–193, 2018 (cit. on p. 4).

[19] M. Ohrelius, M. Berg, R. Wreland Lindström and G. Lindbergh, "Lifetime limitations in multi-service battery energy storage systems," *Energies*, vol. 16, no. 7, p. 3003, 2023 (cit. on p. 4).

[20] B. Ellis, C. White and L. Swan, "Degradation of lithium-ion batteries that are simultaneously servicing energy arbitrage and frequency regulation markets," *Journal of Energy Storage*, vol. 66, p. 107 409, 2023 (cit. on p. 4).

[21] J. Groot, *State-of-health estimation of Li-ion batteries: Ageing models*. Chalmers University of Technology, 2014 (cit. on p. 4).

[22] J. Schmalstieg, S. Käbitz, M. Ecker and D. U. Sauer, "From accelerated aging tests to a lifetime prediction model: Analyzing lithium-ion batteries," in *2013 World electric vehicle symposium and exhibition (EVS27)*, IEEE, 2013, pp. 1–12 (cit. on p. 4).

[23] M. Petit, E. Prada and V. Sauvant-Moynot, "Development of an empirical aging model for li-ion batteries and application to assess the impact of vehicle-to-grid strategies on battery lifetime," *Applied energy*, vol. 172, pp. 398–407, 2016 (cit. on p. 4).

[24] E Sarasketa-Zabala, I Gandiaga, E Martinez-Laserna, L. Rodriguez-Martinez and I Villarreal, "Cycle ageing analysis of a lifepo4/graphite cell with dynamic model validations: Towards realistic lifetime predictions," *Journal of Power Sources*, vol. 275, pp. 573–587, 2015 (cit. on p. 4).

[25] P Ramadass, B. Haran, R. White and B. N. Popov, "Mathematical modeling of the capacity fade of li-ion cells," *Journal of power sources*, vol. 123, no. 2, pp. 230–240, 2003 (cit. on p. 4).

[26] J. Park, W. A. Appiah, S. Byun, D. Jin, M.-H. Ryou and Y. M. Lee, "Semi-empirical long-term cycle life model coupled with an electrolyte depletion function for large-format graphite/lifepo4 lithium-ion batteries," *Journal of Power Sources*, vol. 365, pp. 257–265, 2017 (cit. on p. 4).

[27] P. Arora, M. Doyle and R. E. White, "Mathematical modeling of the lithium deposition overcharge reaction in lithium-ion batteries using carbon-based negative electrodes," *Journal of The Electrochemical Society*, vol. 146, no. 10, p. 3543, 1999 (cit. on p. 4).

[28] F. Single, A. Latz and B. Horstmann, "Identifying the mechanism of continued growth of the solid-electrolyte interphase," *arXiv preprint arXiv:1812.03841*, 2018 (cit. on pp. 4, 12).

[29] L. von Kolzenberg, A. Latz and B. Horstmann, "Solid–electrolyte interphase during battery cycling: Theory of growth regimes," *ChemSusChem*, vol. 13, no. 15, pp. 3901–3910, 2020 (cit. on p. 4).

[30] F. Single, B. Horstmann and A. Latz, "Revealing SEI Morphology: In-Depth Analysis of a Modeling Approach," *Journal of The Electrochemical Society*, vol. 164, no. 11, E3132–E3145, 2017, ISSN: 0013-4651. DOI: 10.1149/2.0121711jes (cit. on p. 4).

[31] X. G. Yang, Y. Leng, G. Zhang, S. Ge and C. Y. Wang, "Modeling of lithium plating induced aging of lithium-ion batteries: Transition from linear to nonlinear aging," *Journal of Power Sources*, vol. 360, pp. 28–40, 2017, ISSN: 03787753. DOI: 10.1016/j.jpowsour.2017.05.110 (cit. on pp. 4, 14).

[32] S. Hein, T. Danner and A. Latz, "An electrochemical model of lithium plating and stripping in lithium ion batteries," *ACS Applied Energy Materials*, vol. 3, no. 9, pp. 8519–8531, 2020 (cit. on p. 4).

[33] J. Keil and A. Jossen, "Electrochemical modeling of linear and nonlinear aging of lithium-ion cells," *Journal of The Electrochemical Society*, vol. 167, no. 11, p. 110 535, 2020 (cit. on p. 4).

[34] S. E. O'Kane, I. D. Campbell, M. W. Marzook, G. J. Offer and M. Marinescu, "Physical origin of the differential voltage minimum associated with lithium plating in li-ion batteries," *Journal of The Electrochemical Society*, vol. 167, no. 9, p. 090 540, 2020 (cit. on p. 4).

[35] S. E. O'Kane, W. Ai, G. Madabattula *et al.*, "Lithium-ion battery degradation: How to model it," *Physical Chemistry Chemical Physics*, vol. 24, no. 13, pp. 7909–7922, 2022 (cit. on pp. 4, 9, 14).

[36] A. A. Wang, S. E. J. O'Kane, F. B. Planella *et al.*, "Review of parameterisation and a novel database (liiondb) for continuum li-ion battery models," *Progress in Energy*, vol. 4, no. 3, p. 032 004, 2022. DOI: 10.1088/2516-1083/ac692c. [Online]. Available: https://dx.doi.org/10.1088/2516-1083/ac692c (cit. on p. 4).

[37] H. D. Abruña, Y. Kiya and J. C. Henderson, "Batteries and electrochemical capacitors," *Phys. Today*, vol. 61, no. 12, pp. 43–47, 2008 (cit. on p. 8).

[38] P. G. Kitz, M. J. Lacey, P. Novák and E. J. Berg, "Operando investigation of the solid electrolyte interphase mechanical and transport properties formed from vinylene carbonate and fluoroethylene carbonate," *Journal of Power Sources*, vol. 477, p. 228 567, 2020 (cit. on p. 8).

[39] J. B. Goodenough and Y. Kim, "Challenges for rechargeable li batteries," *Chemistry of materials*, vol. 22, no. 3, pp. 587–603, 2010 (cit. on p. 8).

[40] M. Doyle, Newman J and T. F. Fuller, "Modeling of galvanostatic charge and discharge of the lithium/polymer/insertion cell," *Journal of the Electrochemical Society*, vol. 140, no. 6, pp. 1526–1533, 1993 (cit. on p. 9).

[41] M. Doyle, T. F. Fuller and J. Newman, "The importance of the lithium ion transference number in lithium/polymer cells," *Electrochimica Acta*, vol. 39, no. 13, pp. 2073–2081, 1994 (cit. on p. 9).

[42] T. F. Fuller, M. Doyle and J. Newman, "Simulation and optimization of the dual lithium ion insertion cell," *Journal of the Electrochemical Society*, vol. 141, no. 1, p. 1, 1994 (cit. on p. 9).

[43] C. R. Birkl, M. R. Roberts, E. McTurk, P. G. Bruce and D. A. Howey, "Degradation diagnostics for lithium ion cells," *Journal of Power Sources*, vol. 341, pp. 373–386, 2017, ISSN: 03787753. DOI: 10.1016/j.jpowsour.2016.12.011 (cit. on pp. 11, 15).

[44] X. G. Yang, Y. Leng, G. Zhang, S. Ge and C. Y. Wang, "Modeling of lithium plating induced aging of lithium-ion batteries: Transition from linear to nonlinear aging," *Journal of Power Sources*, vol. 360, pp. 28–40, 2017, ISSN: 03787753. DOI: 10.1016/j.jpowsour.2017.05.110 (cit. on p. 11).

[45] J. M. Reniers, G. Mulder and D. A. Howey, "Review and Performance Comparison of Mechanical-Chemical Degradation Models for Lithium-Ion Batteries," *Journal of The Electrochemical Society*, vol. 166, no. 14, A3189–A3200, 2019, ISSN: 0013-4651. DOI: 10.1149/2.0281914jes. [Online]. Available: https://ecsarxiv.org/zdwsu/ (cit. on p. 11).

[46] J. S. Edge, S. O'Kane, R. Prosser *et al.*, "Lithium ion battery degradation: What you need to know," *Physical Chemistry Chemical Physics*, vol. 23, no. 14, pp. 8200–8221, 2021 (cit. on pp. 11, 15).

[47] S. Wang, K. Yang, F. Gao, D. Wang and C. Shen, "Direct visualization of solid electrolyte interphase on li 4 ti 5 o 12 by in situ afm," *Rsc Advances*, vol. 6, no. 81, pp. 77 105–77 110, 2016 (cit. on p. 11).

[48] E. Peled, "The electrochemical behavior of alkali and alkaline earth metals in nonaqueous battery systems—the solid electrolyte interphase model," *Journal of The Electrochemical Society*, vol. 126, no. 12, p. 2047, 1979 (cit. on p. 11).

[49] S.-H. Kang, D. Abraham, A Xiao and B. Lucht, "Investigating the solid electrolyte interphase using binder-free graphite electrodes," *Journal of Power Sources*, vol. 175, no. 1, pp. 526–532, 2008 (cit. on p. 11).

[50] D. Li, D. Danilov, Z. Zhang, H. Chen, Y. Yang and P. H. Notten, "Modeling the sei-formation on graphite electrodes in lifepo4 batteries," *Journal of The Electrochemical Society*, vol. 162, no. 6, A858, 2015 (cit. on p. 12).

[51] J. Bates and D. Leibling, "Spaced out - perspectives on parking policy," RAC, Tech. Rep., 2012 (cit. on p. 12).

[52] Q. Liu, C. Du, B. Shen *et al.*, "Understanding undesirable anode lithium plating issues in lithium-ion batteries," *RSC advances*, vol. 6, no. 91, pp. 88 683–88 700, 2016 (cit. on p. 12).

[53] N. Legrand, B. Knosp, P. Desprez, F. Lapicque and S. Raël, "Physical characterization of the charging process of a Li-ion battery and prediction of Li plating by electrochemical modelling," *Journal of Power Sources*, vol. 245, pp. 208–216, 2014, ISSN: 03787753. DOI: 10.1016/j.jpowsour.2013.06.130. [Online]. Available: https://www.sciencedirect.com/science/article/pii/S0378775313011373 (cit. on p. 13).

[54] I. Laresgoiti, S. Käbitz, M. Ecker and D. U. Sauer, "Modeling mechanical degradation in lithium ion batteries during cycling: Solid electrolyte interphase fracture," *Journal of Power Sources*, vol. 300, pp. 112–122, 2015, ISSN: 03787753. DOI: 10.1016/j.jpowsour.2015.09.033 (cit. on p. 14).

[55] R. Jung, M. Metzger, F. Maglia, C. Stinner and H. A. Gasteiger, "Oxygen release and its effect on the cycling stability of linixmnycozo2 (nmc) cathode materials for li-ion batteries," *Journal of The Electrochemical Society*, vol. 164, no. 7, A1361, 2017 (cit. on p. 15).

[56] M. Dubarry and B. Y. Liaw, "Identify capacity fading mechanism in a commercial lifepo4 cell," *Journal of power sources*, vol. 194, no. 1, pp. 541–549, 2009 (cit. on p. 15).

[57] N Ding, J Xu, Y. Yao *et al.*, "Determination of the diffusion coefficient of lithium ions in nano-si," *Solid State Ionics*, vol. 180, no. 2-3, pp. 222–225, 2009 (cit. on p. 17).

[58] B. Lu, Y. Song, Q. Zhang, J. Pan, Y.-T. Cheng and J. Zhang, "Voltage hysteresis of lithium ion batteries caused by mechanical stress," *Physical Chemistry Chemical Physics*, vol. 18, no. 6, pp. 4721–4727, 2016 (cit. on p. 17).

[59] L. St, S. Wold *et al.*, "Analysis of variance (anova)," *Chemometrics and intelligent laboratory systems*, vol. 6, no. 4, pp. 259–272, 1989 (cit. on p. 19).

[60] A. Bessman, R. Soares, O. Wallmark, P. Svens and G. Lindbergh, "Aging effects of ac harmonics on lithium-ion cells," *Journal of Energy Storage*, vol. 21, pp. 741–749, 2019 (cit. on pp. 25, 31).

[61] J. M. Chambers, A. E. Freeny and R. M. Heiberger, "Analysis of Variance; Designed Experiments," in *Statistical Models in S*, Routledge, 2018, pp. 145–193, ISBN: 9780203738535. DOI: 10.1201/9780203738535-5 (cit. on p. 31).

[62] A. J. Smith, P. Svens, M. Varini, G. Lindbergh and R. W. Lindström, "Expanded In Situ Aging Indicators for Lithium-Ion Batteries with a Blended NMC-LMO Electrode Cycled at Sub-Ambient Temperature," en, *Journal of The Electrochemical Society*, vol. 168, no. 11, p. 110 530, Nov. 2021, Publisher: IOP Publishing, ISSN: 1945-7111. DOI: 10.1149/1945-7111/ac2d17. [Online]. Available: https://dx.doi.org/10.1149/1945-7111/ac2d17 (visited on 16/03/2023) (cit. on p. 37).

[63] J. Sturm, A. Rheinfeld, I. Zilberman *et al.*, "Modeling and simulation of inhomogeneities in a 18650 nickel-rich, silicon-graphite lithium-ion cell during fast charging," *Journal of Power Sources*, vol. 412, pp. 204–223, 2019 (cit. on pp. 39, 40).